From THE DEPARTMENT OF CLINICAL NEUROSCIENCE
Karolinska Institutet, Stockholm, Sweden

DEVELOPMENT OF NOVEL PET RADIOLIGANDS FOR VISUALIZING BETA CELL MASS AND AMYLOID PLAQUES

Mahabuba Jahan

Karolinska Institutet

Stockholm 2016

Cover Illustration:

From left to right; i) whole body PET scans in pigs using radioligands [^{18}F]FE-DTBZ (left) and [^{18}F]FE-DTBZ-d4 (right) ii) transaxial PET/CT fusion image in pig where white and red arrows indicate pancreas and hepatic tissues uptake iii) autoradiogram and insulin staining of consecutive human pancreas section iii) whole hemisphere coronal autoradiographs of AD (left) and non-AD (right) subjects.

Published by Karolinska Institutet.

Printed by Eprint AB 2016

ISBN 978-91-7676-362-9

Development of novel PET radioligands for visualizing Beta Cell Mass and Amyloid Plaques

Thesis for doctoral degree (Ph.D.)

By

Mahabuba Jahan

Principal Supervisor:

Professor Christer Halldin
Karolinska Institutet
Dept. of Clinical Neuroscience

Co-supervisor(s):

Associate Professor Olof Eriksson
Uppsala Universitet
Dept. of Medicinal Chemistry

Dr. Peter Johnström
AstraZeneca Translational Science Center
Karolinska Institutet
Dept. of Clinical Neuroscience

Opponent:

Associate Professor Dirk Bender
Aarhus University
Dept. of Nuclear Medicine & PET research
Aarhus, Denmark.

Examination Board:

Professor MD Mikael Rydén
Karolinska Institutet
Dept. of Medicine
Huddinge, Sweden.

Professor Franklin Aigbirhio
Cambridge University
Dept. of Clinical Neuroscience
Cambridge, UK.

Associate Professor Luke Odell
Uppsala Universitet
Dept. of Medicinal Chemistry
Uppsala, Sweden.

Goals aren't a matter of luck; they're a matter of persistence. Nothing worth achieving happens overnight.

This thesis is dedicated

To the loving memory of my father, for your endless support and strong belief in me,

To my mother, for giving me the light of this world,

To my husband, for loving me exactly who I am,

To my adorable daughter, for giving me a new meaning in life.

ABSTRACT

The aim of the thesis was twofold. The first aim was to radiolabel small molecules by using carbon-11 and fluorine-18 for visualising beta cell mass (BCM) in the pancreas by PET. Diabetes Mellitus (DM) is a chronic metabolic disorder that results from an absolute or relative lack of BCM of endocrine pancreas. The lack of an adequate non-invasive imaging PET probe prevents detailed examination of beta cell loss during onset and progression of DM as well as development of novel treatments and islets transplantation progress. The second aim of the thesis was to radiolabel peptide molecules with fluorine-18 to visualise beta amyloid in Alzheimer's disease (AD) brain. AD is a chronic, progressive neurodegenerative disorder. Brain penetration study of a labelled peptide, specific for beta amyloid that can cross blood-brain-barrier (BBB), is important to gain knowledge about the fate of the molecule as a diagnostic probe.

A series of three novel radioligands for BCM imaging has been developed in this thesis. In paper I, a vesicular monoamine transporter type 2 (VMAT2) specific radioligand [^{18}F]FE-DTBZ-d4 was synthesised in two steps. First step is the nucleophilic [^{18}F]fluorination to produce deuterated-[^{18}F]fluoroethylbromide followed by the *O*-alkylation of desmethyl-DTBZ precursor to produce [^{18}F]FE-DTBZ-d4. The *in vivo* pharmacokinetics (PK) studies in pigs by PET/CT demonstrated reduced *in vivo* defluorination; therefore, it may be an improved potential candidate for imaging VMAT2 dense tissue i.e. islets transplantation in proximity to cortical bone structure. In Paper II, a glucokinase (GK) specific radioligand, [^{11}C]AZ12504948, was synthesised in one step via alkylation of *O*-desmethyl precursor using [^{11}C]methyl iodide. Both *in vitro* and *in vivo* (pig and monkey) studies with [^{11}C]AZ12504948 for imaging GK in the pancreas and liver indicated low specificity. Increased target specificity is required for further progress in GK imaging using PET radioligands. In Paper III, a radioligand for G-protein coupled receptor 44 (GPR44), [^{11}C/^{3}H]AZ Compound X, was synthesised via *S*-methylation of sodium sulfinate salt in one step using [^{11}C/^{3}H]methyl iodide. *In vitro* binding of the radioligand, evaluated by autoradiography (ARG) on human and rat pancreatic tissues, confirmed higher specific binding in islets of human pancreatic tissue and no measurable binding in rat pancreas, which is devoid of GPR44. These studies indicate that the radioligand has suitable properties for beta cell imaging with high potential for further preclinical and clinical evaluation.

Three novel D-peptides were radiolabelled with fluorine-18 ([^{18}F]ACI-87, [^{18}F]ACI-88, [^{18}F]ACI-89) by using prosthetic group *N*-succinimidyl-*4*-[^{18}F]fluorobenzoate, [^{18}F]SFB, with epsilon (ε)-amino groups of lysine residues of peptide precursors in two steps. First step is the synthesis of [^{18}F]SFB followed by the addition of [^{18}F]SFB via acylation to the peptide molecule. Trimethylammonium salt [$N(CH_3)_3^+$] precursor for synthesising [^{18}F]SFB as well as the reference standard SFB were synthesised with good yields. Three ^{19}F-peptide reference standards were also synthesised by using SFB. Preliminary ARG measurements were performed in AD and control human brains. ARG demonstrated higher radioligand uptake in the AD brain compared to age-matched control brain, which makes them potential for further use in *in vivo* testing by PET. However, preliminary PET (*in vivo*) studies in cynomolgus monkey brain, using these ^{18}F-D-peptides, confirmed too low BBB penetration, making them unsuitable for further use as *in vivo* PET probes.

LIST OF THESIS PUBLICATIONS

I. Decreased defluorination using the novel beta-cell imaging agent [^{18}F]FE-DTBZ-d4 in pigs examined by PET. *European Journal of Nuclear Medicine and Molecular Imaging Research* **2011**, 357-363.
***Jahan M,** *Eriksson O, Johnström P, Korsgren O, Sundin A, Johansson L, Halldin C.

II. Synthesis and Biological Evaluation of [^{11}C]AZ12504948; a novel tracer for imaging of glucokinase in pancreas and liver. *Nuclear Medicine and Biology*, **2015**, 387-394.
***Jahan M,** Johnström P, Nag S, Takano A, Korsgren O, Sundin A, Johansson L, Halldin C, Eriksson O.

III. Radiosynthesis and preliminary evaluation of novel radioligand for GPR44 using autoradiography on postmortem pancreas for visualizing Beta Cells. *(Manuscript)*.
***Jahan M**, Selvaraju RK, Johnström P, Svedberg M, Schou M, Jia Z, Korsgren O, Eriksson O, Halldin C.

IV. Fluorine-18 labeling of three novel D-Peptides by conjugation with *N*-succinimidyl-4-[^{18}F]-fluorobenzoate and preliminary examination by post mortem whole hemisphere human brain autoradiography. *Nuclear Medicine and Biology*, **2012**, 315-323.
***Jahan M**, Nag S, Krasikova R, Weber U, Muhs A, Pfeifer A, Spenger C, Willbold D, Gulyás B, Halldin C.

Related publication which is not part of the thesis:

In vivo and *in vitro* characterization of [^{18}F]-FE-(+)-DTBZ as a tracer for beta-cell mass. *Nuclear Medicine and Biology* **2010**, 357-63.
*Eriksson O, **Jahan M**, Johnström P, Korsgren O, Sundin A, Halldin C, Johansson L.

CONTENTS

List of abbreviations

^{11}C	Radioactive, neutron deficient isotope of carbon
^{18}F	Radioactive, neutron deficient isotope of fluorine
^{13}N	Radioactive, neutron deficient isotope of *nitrogen*
^{15}O	Radioactive, neutron deficient isotope of oxygen
BCI	Beta cell imaging
BCM	Beta cell mass
CT	Computed tomography
MRI	Magnetic resonance tomography
$[^{11}C]CH_4$	$[^{11}C]$Methane
$[^{11}C]CH_3I$	$[^{11}C]$Methyl iodide
$[^{11}C]CH_3OTf$	$[^{11}C]$Methyl triflate
DTBZ	Dihydrotetrabenazine
VMAT2	Vesicular monoamine transporter 2
ARG	Autoradiography
T1DM	Type 1 diabetes mellitus
T2DM	Type 2 diabetes mellitus
EOB	End of bombardment (Irradiation)
EOS	End of synthesis
Cyclotron	Particle accelerator
MeV	Mega electron volt
Carrier	Nonradioactive form of radioligand/radiotracer
α	Alpha particle, positive helium ion (He^{2+})
Bq	Becquerel, SI derived unit of radioactivity
Hot-Cell	Lead-shielded containment box
HPLC	High performance liquid chromatography
HRRT	High resolution research tomography
Kryptofix ($K_{2.2.2.}$)	4, 7, 13, 16, 21, 24-hexaoxa-1, 10-diazabicyclo [8.8.8]-hexacosane
Lipophilic	Non-polar, tendency to not dissolve well in water
Hydrophilic	Polar, tendency to dissolve well in water
LogP	Logarithm of partition coefficient octanol/water
MeCN	Acetonitrile
DMF	Dimethylformamide
DMSO	Dimethyl sulfoxide
RCY	Radiochemical yield
RT	Room temperature
SRA	Specific radioactivity
ROI	Region of interest
SUV	Standard uptake value
$T_{1/2}$	Half-life

BP	Binding potential
PVE	Partial volume effect
PTC	Phase transfer catalysts
AD	Alzheimer's disease
In vitro	"in flask" i.e. in the test tube
In vivo	"in life" i.e. in the organism
ID	Injected dose
B_{max}	Binding maximum i.e. total receptor density
K_d	Dissociation constant
LC-MS	Liquid chromatography-mass spectrometry
I.V.	Intravenous injection
p.i.	Post injection
MIP	Maximum intensity projection
PBS	Phosphate buffer saline
SPE	Solid phase extraction
RM	Reaction mixture
PET	Positron emission tomography
β –Cells	Beta cells

1 INTRODUCTION

Henri Becquerel discovered natural radioactivity in 1896, immediately after the discovery of X-rays by W. C. Röntgen. The research on radioactivity was further investigated by Marie Curie and her husband Pierre Curie, and they were able to isolate natural radioactive elements in 1898. The discovery of this natural radioactivity had great scientific sensation at that time and still has tremendous implications in our lives. Suddenly, several new elements were discovered that emitted different types of radiation but were chemically identical with already known elements, and to solve the problem, the concept of isotopes (Greek; iso=same, tope=place) was introduced by Soddy in 1913. Almost at the same time (1913), the practical implication of the isotopic theory was demonstrated by George de Hevesy and his colleagues in the field of inorganic chemistry[1]. De Hevesy was also the first one to use the radioactive tracer technique in biology by using the radioisotope lead-212, ^{212}Pb, to investigate lead uptake in plants[2] and radiotracer phosphorous-32, ^{32}P, to study the tracer distribution in rats[3]. So far, for the radioactive nuclides used in these studies, nature was the supplier.

1.1 MOLECULAR IMAGING USING PET

New era of tracer technique using radiation started with the discovery of artificially induced radioactivity by the couple Irene Curie and Frédéric Joliot in 1934. They demonstrated the production of artificial radioactive isotope (^{30}P) with short half-life ($t_{1/2}$ =3.15 min), by bombarding aluminium foil with alpha particles via the nuclear reaction ^{27}Al(α,n)^{30}P[4]. They also suggested that it was possible to produce similar radioactive elements with different nuclear reactions by using different bombarding particles, such as protons, neutrons and deuterons[4]. This hypothesis was proved to be true by Ernest Lawrence et al. in Berkeley, California who had already started working with accelerating particles between two D-shaped magnets, called a cyclotron, to produce high energy protons and deuterons that could bombard elements to explore the nature of the atomic nucleus[5]. In the same year (1934), with the progression of increased size of the cyclotron, Lawrence and Livingston et al. could produce large quantities of artificial short lived radioisotopes, including carbon-11, nitrogen-13, oxygen-15 and fluorine-18[6], which have subsequently been proved to have great significance in biomedical science, research and clinical practice today.

The term molecular imaging can be defined as the non-invasive visualisation of biological processes *in vivo* at the molecular or cellular levels using specific imaging

tracers[7,8]. Positron emission tomography (PET) is a non-invasive molecular imaging (*in vivo*) technique that allows for the localisation of a molecule labelled with positron emitting nuclides[9], based on the detection of positron annihilation radiation and subsequently processing of raw data onto an image[10, 11]. PET was developed at the end of 1970s[12-14], but the full potential of the technique was not acknowledged outside the scientific community until 1990s[15]. Numerous studies with ^{18}F-labelled deoxyglucose ([^{18}F]FDG), developed by Ido et al.[16], using PET scanners demonstrated how accumulation of [^{18}F]FDG in cancerous lesions helped by giving a solution for many problems by means of diagnosis and prognosis with cancer patients[17-20]. Nowadays, PET is frequently used for early detection, characterisation, real time monitoring of diseases as well as investigating the effectiveness of therapeutic drugs[7]. PET can provide the molecular interactions between the tracer molecule and the biological target, e.g. a protein, transporter, enzyme function and inhibition, metabolism and general biochemical function. PET has become a powerful functional imaging tool, and the most used application of PET imaging is implemented in oncology[21], neuroscience[22, 23] and cardiovascular diseases[24, 25].

Another major utility of PET imaging is to understand and facilitate drug action and development[26-28], which can be investigated in two ways. First, actual drugs or new drug candidates can be radiolabelled, and pharmacokinetics of the drug such as absorption, distribution, metabolism and excretion (ADME) can be studied by PET[29, 30] using the microdose concept i.e. maximum doses of ≤100 µg or 1/100th of the therapeutic doses are used[31]. Based on early *in vivo* PET studies, costly failures[32] of 'go' or 'no go' decisions can be made in very early stages of drug development. The second area is to evaluate pharmacodynamics or dose finding studies through receptor occupancy[30, 33, 34]. Several well characterised PET radioligands have been used to measure receptor occupancies of antipsychotic drugs[35-37] and the relationship between receptor occupancy, clinical usefulness and side-effects[38-40].

1.2 HOW DOES PET WORK

PET imaging agents are radiolabelled with positron emitting radionuclides, such as ^{11}C, ^{18}F, ^{13}N and ^{15}O, which are the radioisotopes of the stable natural elements of ^{12}C, ^{19}F, ^{14}N and ^{16}O, respectively, and they decay (with different half-lives, Table 1) by the emission of a positively charged particle, called positron. For example, ^{11}C-radioisotope decays by positron emission and forms the stable nuclide boron, ^{11}B. When the labelled compound (radiotracer or radioligand) is administered intravenously *in vivo*, the emitting positron from the radio-

nuclide travels a short distance in the surrounding matter or wet tissue where it collides with its antiparticle, an electron, and consequently annihilates. This annihilation results in emission of two 511 KeV gamma rays (photons), which travel approximately 180˚ apart from each other and are detected by an array of surrounding gamma ray detectors of the PET scanning device (Figure 1). Photons, which are registered only in pairs (within few nanoseconds) by the PET scanner, are considered to be originated from the same source and thereby, the position of the positron. The distribution of the radioactivity is then visualised and quantified as a function of time[41] after reconstruction[11] and appropriate correction for scatter and random coincidences. The distance travelled by the positron in the surrounding tissue before annihilation is known as positron range. The emitted positron energy is different for each radionuclide, which determines the travel length of the positron before annihilation (Table 1). The larger the positron energy, the longer the average distance the positron travels before annihilation and the larger the loss in spatial resolution[42].

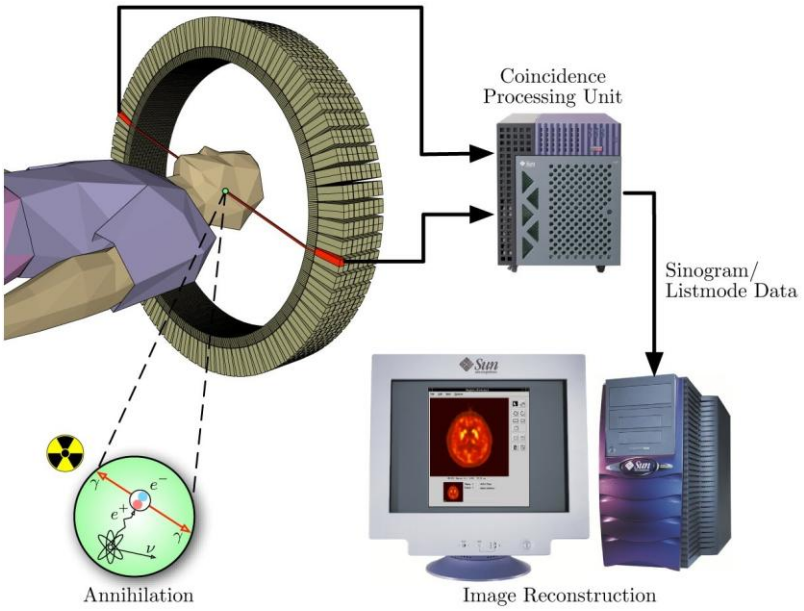

Figure 1. Schematic diagram representing acquisition and reconstruction of PET images.[43]

Table 1. Physical properties of commonly used positron emitting radionuclides (the shorter the half-life, the higher the SRA value).

Radionuclide	Half-life ($T_{1/2}$=min)	Maximum Energy (MeV)	Max linear range in water (mm)	Theoretical SRA (GBq/µmol)
^{15}O	2.04	1.72	8.20	3.4×10^{6}
^{13}N	9.96	1.19	5.39	7.0×10^{5}
^{11}C	20.4	0.96	4.12	3.4×10^{5}
^{68}Ga	67.6	1.899	9	1×10^{5}
^{18}F	109.7	0.635	2.39	6.3×10^{4}

1.3 DEVELOPMENT OF PET RADIOLIGANDS

The real challenge in PET molecular imaging is the search for the 'optimal' ligand. This development requires a multidisciplinary approach regarding; molecular target and radionuclide selection, organic synthesis, production of radionuclide, radiolabelling, quality control, *in vitro* and *in vivo* evaluation, detection of radiation, tomographic reconstruction, and finally, the application of a series of corrections to provide image representative of the ligand distribution in the live animals or human. In order to be able to develop a successful innovative radioligand, some important parameters need to be taken under consideration[27, 44] which are discussed below.

1.3.1 Time aspects

In syntheses using short-lived radionuclides, time is more important than in conventional synthetic work[45-47]. The ^{11}C decay curve and the yield curves (Figure 2) indicate the importance of optimising synthesis time in relation to the labelled product formation. The length of the radiosynthesis and purification time should be as short as possible, and the radionuclide incorporation in the synthetic route should be as late as possible due to short half-lives of the radionuclides. To minimise the losses of radioactivity due to radioactive decay, work up procedure should be optimised to maximise radiochemical yield (RCY) and specific radioactivity (SRA)[47], for example, solid phase extraction (SPE) purification is more desirable than high performance liquid chromatography (HPLC), microwave heating more than conventional heating[47, 48] to speed up the process. In radiochemistry, it is also important to remember that the labelled precursors (^{11}C or ^{18}F) are produced in very low amounts; therefore, by increasing the amount of non-labelled reactants/precursor (10^3-10^4 fold of labelled precursor), one can increase the reaction rate and rapid formation of the radiolabelled product.

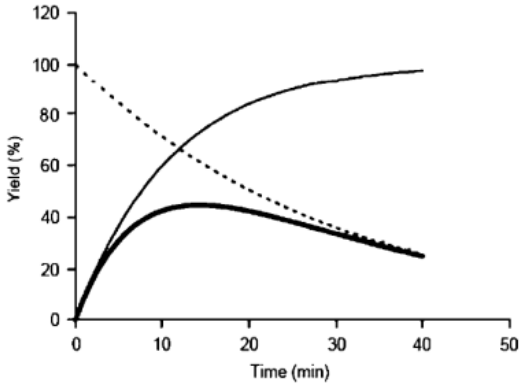

Figure 2. Decay curve for ^{11}C (dotted line), chemical yield in a hypothetical chemical reaction involving only stable nuclides ^{12}C (solid line), and decay-corrected RCY using same reaction but including ^{11}C-(bold-line)[7].

1.3.2 Binding affinity

Binding affinity means how tightly a ligand binds to its target e.g. receptor, transporter or enzyme. Affinity is denoted as K_d and it can be expressed as the inverse equilibrium dissociation constant i.e. $K_d=k_{off}/k_{on}$. The required affinity mainly depends on the concentration of binding sites (B_{max}) in the region of interest. A low concentration of binding sites means the affinity of the radioligand must be high (low K_d). Since sites are easier to saturate, the SRA of the ligand needs to be sufficiently high. It is preferable if B_{max} is higher than K_d by one order of magnitude, i.e. if B_{max} exists at nanomolar concentration, K_d should have subnanomolar concentration for good image contrast[44]. Typically, the most successful ligand have subnanomolar or low nanomolar affinity to the target of interest *in vitro*. A binding potential (BP), ratio of B_{max}/K_d, value > 5-10 can be used as a rule of thumb[49, 50] the higher the ratio, the more sensitive the signal.

1.3.3 Specificity, selectivity and sensitivity

The characteristic of a binding site or receptor to be activated only by a single molecule or class of molecules is known as specificity. The selectivity can be defined as relative affinity of the radioligand to the region of interest over other binding sites. If the biological target is well separated from the nonbinding site, then ligands with low selectivity can also be considered. High specificity and selectivity is required for low dense receptor site to get good signal to noise ratio. Many radioligands fail in early stages due to high non-target binding i.e. binding to a target or tissue other than the site of interest[51]. The sensitivity is affected by other factors such as kinetics, surrounding-tissue uptake, spatial resolution, data handling, etc.

1.3.4 Lipophilicity

During the development of a new radioligand, lipophilicity (log P) of a molecule plays an important role, since non-specific interaction in addition to the tissue or target increases with increased lipophilicity[49] i.e. specific-to-nonspecific binding ratios. For example, high lipophilic molecules tend to bind to plasma protein, thus, resulting in a reduction of free fraction in the blood and reduced delivery of the ligand to the specific sites. In contrast, molecules with low lipophilicity have higher water solubility, thus, faster clearance through the kidneys and limited blood-brain-barrier (BBB) penetration. Therefore, to find an optimal log P value is a challenge during radioligand development. The

recommended log P value to cross the BBB is between 1 and 3.5, preferably less than 3[52]. Lipophilicity can influence a drug's or ligand's pharmacokinetics i.e. ADME[53]. For example, high lipophilic compound is eliminated mostly via the liver, thus, confounding PET images of nearby tissues, e.g. in this thesis, the pancreas. Due to high uptake or nonspecific binding near gastrointestinal tract, delineation of pancreas is troublesome, consequently affecting the specific uptake. However, lipophilicity and thereby elimination path can be altered by designing the ligand to be more hydrophilic upon addition of various amide linkers[54] or by incorporation of a fluorine atom; replacement of a hydrogen atom by fluorine in an aliphatic position generally decreases the lipophilicity, while substitution in an aryl group increases the lipophilicity[55]. Lipophilicity can be calculated theoretically in advance by using computer programs[56] or practically by the logarithm of the partition coefficient ratio between octanol and water/buffer at physiological pH.

1.3.5 Specific radioactivity (SRA)

SRA is defined as the concentration of a radioactive material in a sample, and is expressed as the radioactivity of the labelled compound divided by the molar amount of the compound (Bq/mol). In this thesis, SRA is expressed as GBq/μmol. The higher the SRA, the less the amount of ligand used, consequently, minimising the risk of saturation of the binding sites, as well as less risk of perturbation of the investigated biological system with unlabelled counterpart. For low density receptor binding sites, the SRA of the radioligand is very important and can limit its usefulness as an imaging agent. Even a small amount of injected cold ligand may lead to significant receptor occupancy and decrease the signal-to-noise ratio while possibly inducing pharmacological effects. For receptor-ligand interaction studies, high SRA is required to quantify the number of free receptors followed by drug occupancy. In contrast, for drug distribution studies or labelled endogenous compounds, SRA is not that important. Theoretical SRA values of PET radionuclides are very high, since they have short half-lives (Table 1). Due to isotopic dilution with its stable element, it is impossible to reach the theoretical SRA values with ^{11}C and ^{18}F radioligands. Despite isotopic dilution, the obtained SRA of ^{11}C and ^{18}F radioligand is sufficiently high enough to follow biochemical and physiological processes. For example, in clinical settings with consistent production of the radioligand, [^{11}C]AZ Compound X, with SRA>1000 GBq/μmol on average and in combination with weight of human (60-80 kg), the estimated administered chemical amount of the carrier following injection of 300 MBq would be <0.001 μg/kg [Paper **III**].

1.3.6 Radiolabelling and radiometabolism

The position of the radiolabelling is not critical for *in vitro* studies (e.g. frozen tissue autoradiography), since radioligand metabolism is not expected. In contrast, ligand metabolism occurs throughout *in vivo* PET studies; therefore, the position of the labelling is very important. The PET scanner is unable to distinguish between radiochemical entities, since it can measure only radioactivity. As a result, if a radiometabolite enters the target, it will confound PET images with background radioactivity, which is not associated with the biological process under study; especially if the radiometabolite has some degree of target selectivity[57]. Therefore, a labelling position should be chosen carefully so that it is metabolically stable, preferably during the PET investigation, or, alternatively, labelled metabolites are hydrophilic enough and consequently eliminated quickly. For example, metabolic loss of ^{18}F *in vivo* can be reduced by replacing hydrogen atoms with deuterium[58] (Paper **I** of this thesis) and can change the rate of reaction[59]. The rate of metabolism of a radioligand and the lipophilicity of radiometabolites can be estimated quantitatively using radio-HPLC technique[60]; moreover, radiometabolites can be identified with the help of highly sensitive LC-MS/MS[61, 62] techniques.

1.4 STRATEGIES FOR CARBON-11 LABELLING

As a key element of life, carbon is of special interest for labelling compounds, including endogenous as well as other naturally occurring bio-molecules. Replacement of naturally occurring ^{12}C by ^{11}C does not alter the (bio)chemical properties of a molecule. The choice of radionuclide is ^{11}C for radiolabelling during investigation of drugs for drug development or to measure biochemical processes. Since ^{11}C has short half-life, longitudinal *in vivo* studies can be performed on the same day on the same subject. Many synthetic routes to ^{11}C-compounds are already available (Figure 3) and several others are currently under development. Primary ^{11}C-precursors are mainly [^{11}C]CO_2 and [^{11}C]CH_4, which can be produced by the same nuclear reaction in nitrogen gas targets containing trace amounts of oxygen and hydrogen gas, respectively (Figure 3). Target produced [^{11}C]CO_2 gives lower SRA due to unavoidable isotopic dilution; nonetheless, different secondary ^{11}C-precursors can be prepared from [^{11}C]CO_2 by online or in one-pot procedures, which can give high SRA such as [^{11}C]cyanide ([^{11}C]CN)[63] and [^{11}C]carbon monoxide ([^{11}C]CO)[64, 65]. Secondary ^{11}C-precursors [^{11}C]CH_3I, obtained via gas-phase method[66] from target produced [^{11}C]CH_4, can produce very high SRA (10^4 GBq/μmol)[67] compared to [^{11}C]CO_2.

The most widely used methylating agent [^{11}C]CH_3I, introduced in 1970s[68, 69] was mainly used for methylation on nitrogen, oxygen and sulfur containing nucleophiles with the corresponding desmethyl precursors[44, 47]. [^{11}C]CH_3I can be produced either by the "wet" method or by the "dry" method[70]. Besides [^{11}C]CH_3I, carbon disulfide, [^{11}C]CS_2 was introduced as ^{11}C-labelling reagent for an effective route to synthesise ^{11}C-labelled organosulfur compounds[71], and [^{11}C]methyl triflate, [^{11}C]CH_3OTf[72-74], has been utilised to improve the RCY in ^{11}C-methylations. Recent development of the micro-reactor technology for radiosynthesis has some advantages over conventional laboratory methods such as purer products, higher yields and shorter reaction times due to superior heating and controlled mixing of reagent streams[75, 76]. The formation of carbon-carbon bond (^{11}C-C) via nucleophilic addition of Grignard reagent to [^{11}C]CO_2[77] or via [^{11}C]CN[78, 79] were very popular; however, recently organometallic-mediated ^{11}C-C cross-coupling reactions using Stille, Suzuki or Sonogashira have also emerged[80-83].

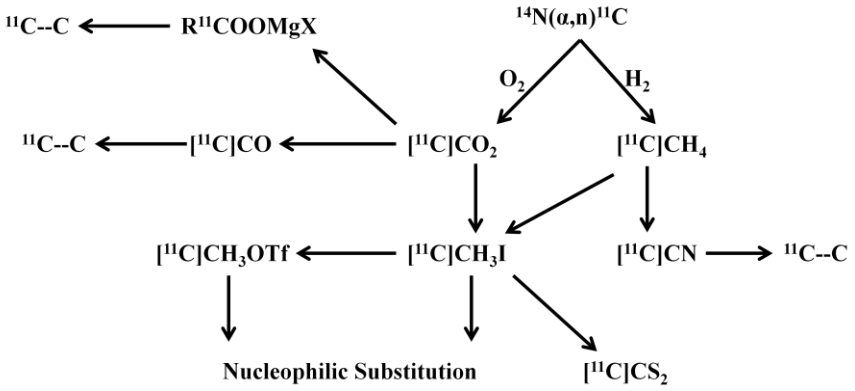

Figure 3. Routes of producing ^{11}C-labelled radiopharmaceuticals.

1.5 STRATEGIES FOR FLUORINE-18 LABELLING

Fluorine atom (F) is generally not a constituent of biomolecules; nevertheless, substitution of hydrogen atom (H) or hydroxyl group (OH) from a molecule with fluorine atom is one of the most commonly used bioisosteric replacements to introduce F in radiochemistry as well as in drug development. The F and H atoms are quite similar in size; therefore, replacement with F for a H would induce minimum steric perturbations[84]. The capability of F atom to form hydrogen bonds due to its high electronegetivity makes it similar to a OH substituent, and due to nature of high-energy bonding with carbon, fluoro-organic pharmaceutical derivatives have improved pharmacological properties[85]. Therefore, almost 20% of the marketed drugs today contain at least one fluorine substituent[86]. Incorporation of

fluorine into drug candidates can increase or decrease the lipophilicity without changing the size of the molecule or changing the rates of *in vivo* absorption, but still allows for the molecule to fit into its binding site[87]. According to radiochemistry point of view, fluorine-18 is a very attractive choice for radionuclide, mainly for two reasons. First, longer half-life ($T_{1/2}$), which allows radiochemist to perform multi-step synthesis as well as permitting transport of ^{18}F-radioligands over considerable distances. It allows PET scans to be acquired over a few hours and consequently following biological processes with quite slow kinetics. Secondly, the mode of decay; fluorine-18 emits quite a low energy positron (maximally 0.635 MeV), which on average has a short path *in vivo* (~2 mm in water) before its annihilation. The positron path is similar to the highest spatial resolution achievable with modern PET cameras today (2–4 mm for a clinical PET camera[88] and 1–2 mm for a μPET camera[89]), therefore. optimal PET image quality compared to other PET radionuclides (Table 1).

Fluorine-18 can be manufactured from the cyclotron in two chemical forms; [^{18}F]fluorine gas (act as an electrophile) or [^{18}F]fluoride (electron-rich and act as a nucleophile), which determines the possible reactions. The principal ^{18}F-labelling methods are restricted to a few and can be divided into these two ways: electrophilic and nucleophilic substitution.

1.5.1 Electrophilic substitution

For electrophilic ^{18}F-labelling reactions, carrier-added (c.a.) [^{18}F]fluorine ([^{18}F]F_2) gas is used as electrophile and can be produced directly from the target. Two different types of nuclear reactions are available for producing elemental [^{18}F]F_2; ^{20}Ne(d,α)^{18}F[90-92] and $^{18}O_2$(p,n)^{18}F[93, 94]. In both cases, produced ^{18}F is adsorbed on the target walls so that an addition of elemental F_2 to the target gas is mandatory to extract the radioactivity; therefore, low SRA is obtained. The most common and practical process for producing [^{18}F]F_2 is ^{20}Ne(d,α)^{18}F reaction even though higher RCY and SRA of [^{18}F]F_2 is achieved from $^{18}O_2$ target using $^{18}O_2$(p,n)^{18}F reaction (since two consecutive irradiations are necessary)[94, 95]. Electrophilic c.a. radiofluorination is limited to applications where low SRA is accepted such as endogenous compounds. Reported highest SRA in literature, obtained for [^{18}F]F_2, is 2 GBq/μmol[96], which has been improved to ~55 GBq/μmol (for ~7.5 GBq of [^{18}F]F_2) from [^{18}F]F^- produced from a water target[97]. However, high SRA is not only preferable but also mandatory for investigations of low concentration binding sites, e.g. BCM in pancreas, which is why only no carrier added (n.c.a.) [^{18}F]fluoride form has been considered in this thesis.

1.5.2 Nucleophilic substitution

Most of the ^{18}F-labelled radiopharmaceuticals available and clinically used today are obtained from nucleophilic substitution reactions based on n.c.a. [^{18}F]fluoride ([^{18}F]F$^-$), which is directly available from the target. The main reason behind the popularity of using [^{18}F]fluoride is based on getting highest SRA, e.g. 5.2×10^3 GBq/μmol[98]. The nucleophilic ^{18}F is achieved as fluoride ion in aqueous solution from ^{18}O(p,n)^{18}F nuclear reaction and delivered from the target to the hot cell. Due to high charge density of the anion, it is highly hydrated and inactivated for nucleophilic reactions. Therefore, strict exclusion of water is needed using [^{18}F]F$^-$ as a nucleophile. This kind of reaction is also sensitive to the presence of trace amounts of metal ions co-eluting with [^{18}F]F$^-$ from the target[99]. In the presence of Lewis acids, the [^{18}F]F$^-$ has a strong tendency to form complexes and hence will be masked by ions of heavy metals. Moreover, [^{18}F]F$^-$ is very easily protonated, forming hydrogen fluoride and hence becoming unavailable for the next reaction. Therefore, radiolabelling has to take place under aprotic but polar conditions. The [^{18}F]F$^-$ is isolated and separated from the ^{18}O-water as well as metal ions by passing through an anion exchange resin[100]. The retained [^{18}F]F$^-$ is then eluted with an acetonitrile solution of kryptofix$_{2.2.2}$ and potassium carbonate (K_2CO_3); subsequently, water is removed by azeotropic distillation with acetonitrile to produce 'naked' [^{18}F]F$^-$ of high nucleophilicity. The Kryptofix$_{2.2.2}$ (aminopolyether), in combination with K_2CO_3 or oxalate[101], is mainly used as phase transfer catalysts (PTC) for further activation of the [^{18}F]F$^-$ anion. Tetraalkylammonium hydrogencarbonates[102, 103] can also be used as PTC and in some cases, it showed advantages over kryptofix for [^{18}F]F$^-$ activation[104, 105], especially if the precursor is sensitive to basic conditions. In general, nucleophilic substitution with [^{18}F]F$^-$ occurs by heating (>100°C) the dried residue of [^{18}F]F$^-$/ K_2CO_3/kryptofix$_{2.2.2}$ with right precursor, in presence of a polar aprotic solvent such as ACN, DMF, DMSO or *o*-DCB[104].

Nucleophilic substitution reaction with [^{18}F]F$^-$ can be divided further into two categories: i) Direct fluorination (one step) via aliphatic and aromatic substitution and ii) Indirect fluorination (two steps) via ^{18}F-labelled prosthetic group or synthon formation followed by a second reaction, such as alkylation, acylation, etc. The aliphatic nucleophilic substitution reaction proceeds via S_N2-mechanism, where substitution takes place by [^{18}F]F$^-$ ion on a precursor containing appropriate leaving group such as halogens (I, Br and Cl) or sulphonic acid ester groups, e.g. mesylate, tosylate, nosylate, triflate, etc. The nucleophilic aromatic substitution (S_NAr) is of even greater importance for ^{18}F-labelled radiopharmaceuticals due to their greater metabolic stability. This reaction takes place with the presence of activating electron withdrawing group (EWG) in the *ortho* or *para* positions

relative to the leaving group[106, 107]. In particular, substituents with strong electron withdrawing properties such as nitro, cyano, carbonyl and trifluoromethyl groups are suitable for the activation step[108, 109]. Halogens (*F, Cl, Br*), nitro (NO_2) and the trimethylammonium salts [$N(CH_3)_3^+$] show increasing reactivity as the leaving group. The leaving group [$N(CH_3)_3^+$] can be advantageous compared to NO_2 due to better separation of the excess precursor from the final product; however, this precursor can lead to some competitive side reactions that can reduce RCY[110-112]. On the other hand, CN group as EWG might not be suitable, since CN is very sensitive to basic conditions, which can lead to undesired hydrolysis product than the desired radiolabelled product[113].

To avoid the presence of extra activating groups in the precursor molecule, many different approaches have been introduced in the radiochemistry field, such as heteroarenes (pyridine) labelling with ^{18}F in the *ortho* positioned leaving group[114-116]. Introduction and extensive work on labelling of [^{18}F]fluoroarenes using diaryliodonium salts[117, 118] as well iodonium ylides precursor[113, 119] have opened new door for radiochemists to explore a class of compounds that are not possible to synthesise via S_NAr reaction[120].

1.5.3 ^{18}F-Fluorination via prosthetic groups (Papers I and IV)

As mentioned above, indirect method is used in ^{18}F-fluorination via prosthetic group. It means a primary ^{18}F-compound is labelled by direct fluorination as described above (either by aliphatic or aromatic substitution), followed by coupling of ^{18}F-compound i.e. prosthetic group, with a second molecule. Important procedures via prosthetic groups include: [^{18}F]fluoroalkylation[121], [^{18}F]fluoroacylation[122, 123] and [^{18}F]fluoroamidation[124]. Application of prosthetic groups is most common for molecules carrying a protic functional group such as thiol, amino or hydroxyl group.

^{18}F-Fluoroalkyl agents such as [^{18}F]fluoropropyl, ethyl or methyl are synthesised by substitution of halogens or sulfonate esters with n.c.a. [$^{18}F]F^-$ [125, 126]. ^{18}F-Fluoroalkyl agents can be purified very easily via disposable Sep-Pak cartridges or distillation from the reaction mixture[127], as they have low boiling point. This purification process of ^{18}F-fluoroalkyl agents produces more chemically and radiochemically pure product as well as eliminates nonvolatile impurities, thus, increasing the RCY of the second reaction[125, 126, 128, 129]. Well-known aliphatic substitution reactions using ^{18}F-fluoroalkyl agents include [^{18}F]fluorocholine[130], [^{18}F]FET[131] and [^{18}F]β-CFT-FP[132]. In this thesis, in paper **I**, [^{18}F]fluoroethyl was used as prosthetic group to radiolabel the hydroxyl group so that we could use same precursor for both ^{11}C and ^{18}F radiolabelling.

Many methods are available to label proteins and peptides; however, most common methods applied for labelling peptide with ^{18}F is the prosthetic group approach[133]. The advantage of using the prosthetic group approach is that the peptide coupling reaction can be performed under mild conditions, thereby, preserving the integrity of the peptide, especially those that are heat and pH sensitive. The disadvantage is the multiple-step time-consuming synthetic procedure, which is an obstacle for widespread clinical applications. The most commonly used prosthetic groups are *N*-succinimidyl-*4*-[^{18}F]fluorobenzoate, [^{18}F]SFB and [^{18}F]fluorobenzaldehyde [^{18}F]FBA. In this thesis, in Paper **IV**, we have radiolabelled peptides with lysine group; therefore, [^{18}F]SFB has been used for radiolabelling. [^{18}F]SFB is an analogue of Bolton-Hunter reagent developed in 1973 for radioiodination of proteins[134], and later on it has been successfully developed for PET radiolabelling[135-137]. The aromatic fluorine-carbon bond of [^{18}F]SFB is more stable and less sensitive towards hydrolysis. Activated esters of *N*-hydroxysuccinimide are good electrophiles for conjugation to nucleophiles (amines of peptides), in order to form stable amide bonds. Based on all these observations, [^{18}F]SFB was selected even though multiple radiochemical steps were required for its production. If aliphatic defluorination is not a concern, an alternative *N*-succinimidyl-*4*-[^{18}F]fluoromethyl benzoate, analogue to [^{18}F]SFB can be produced in one step from a tosyl or nosyl leaving group[138-140]. The recent discovery and development of [^{18}F]fluoride-aluminum complex (Al^{18}F) to radiolabel peptides also provided a good alternative for simplifying the labelling procedure[141]. Unfortunately, the current procedure for forming Al^{18}F-NOTA complex also requires relatively high temperatures, which has reduced the scope of this method.

1.6 RADIOCHEMICAL PURITY, PURIFICATION AND FORMULATION

Radiochemical purity is defined as the fraction of the radioactive species that is in the desired chemical form. All PET radioligands, whether for human or animal use, need to possess a high level of chemical and radiochemical purity (typically >95%). To isolate radiolabelled probe in highest purity form, reaction mixtures (RM) need to be purified after radiolabelling, from other radioactive by-products as well as from precursor and other reagents used during synthesis. HPLC is the best choice to purify radioligand, while SPE cartridge can be used if other impurities are well separated from the radioligand. Generally, RM contains large amounts of organic solvents (e.g. acetonitrile, DMF, DMSO) and need to be diluted with water or buffer prior to injection on HPLC to avoid excessive peak broadening. The preparative HPLC column should be large enough to efficiently separate the

relatively large mass amount of precursor (typically 0.1–10 mg) from the trace amounts of the PET probe. For ^{18}F-labelling, pre-purification of RM on an in-line SPE column is useful for the elimination of relatively large amounts of un-reacted radioactivity [^{18}F]fluoride[142]. Any organic solvents used in mobile phase during preparative HPLC purification procedure that are not compatible with I.V. injection should be removed either by evaporation or by SPE, followed by desorption with ethanol. This step can be omitted if ethanol is used as an organic modifier in the mobile phase; however, due to high viscosity of ethanol it results in a higher back pressure in comparison with other organic solvents such as acetonitrile or methanol.

The pure radioligand after HPLC purification is formulated by dilution with buffer or salt solution to achieve an isotonic injectable solution[143], which is sterilised by sterile membrane filtration or by autoclave. To prevent radiolysis, scavengers such as ascorbic acid or sodium ascorbate or ethanol can be added[144], and solubilising agents such as Tween-80 can be added to lipophilic radioligand formulations to reduce loss of radioactivity by means of adsorption during sterile filtration as well as in syringes and catheters during injection.

1.7 COMBINE MODALITY (PET/CT)

With the development of a prototype integrated PET/CT scanner, a revolution in medical imaging field occurred in 2000[145]. Lack of a clear anatomical reference frame and relatively low spatial resolution are some of the limitations of PET imaging alone. It is also even more difficult to accurately outline anatomic structure of small organs, such as pancreas, which is situated close to abdominal region, without help of structural imaging methods such as CT. Due to spill over of radioligand uptake from the kidney, liver or gastrointestinal tract (that exhibit higher nonspecific radioligand accumulation) and partial volume effect (PVE), it is nearly impossible to delineate the pancreas on the PET image. This limitation can be overcome by integrating functional and anatomical tissue information obtained by combined PET/CT module, which has increased both accuracy of the interpretation and confidence level of the image analyser. All the *in vivo* studies performed in this thesis were investigated using a hybrid PET/CT scanner.

1.8 DIABETES MELLITUS

The pancreas consists of mainly two tissue types: endocrine and exocrine. Only a small percentage (1–2%) of pancreatic mass (~100 g healthy human pancreas) is accounted for as endocrine tissue, which is scattered heterogeneously in Islets of Langerhans all over the exocrine pancreas. Islets are comprised of four different cell types: alpha, beta, delta and

pancreatic polypeptide (PP)-cells, and among them only beta cells secrete insulin in response to elevated blood glucose levels. In islets, beta cells are the most abundant cells (50–80%), followed by alpha cells (20–30%) and the rest are delta and pp-cells (Figure 4)[146]. The islets are well perfused and small in size (40–300 μm in diameter)[147], and the number of beta cells may vary between healthy subjects[148]. Since beta cells are responsible for maintaining normal glucose levels in the blood, an adequate number of functional pancreatic beta cells are required. The collective beta cell numbers are referred to as beta cell mass (BCM), and the proper release of insulin in response to glucose is referred to as beta cell function (BCF). The loss of beta cells reduces insulin production and consequently causes diabetes. Diabetes mellitus (DM) is a metabolic disorder, characterised by hyperglycemia; moreover, it is one of the major causes of death and disability worldwide. In 2012, 1.5 million people died from diabetes[149], and currently >340 million people are affected which will increase to around 522 million by 2030[150]. Two different forms of diabetes are distinguished based on different pathogenesis: Type 1 (T1DM) or insulin dependent and Type 2 (T2DM) or insulin resistant. BCM is reduced significantly in both type 1 and 2 diabetes patients, compared to non-diabetic individuals. In T1DM, an autoimmune attack against pancreatic beta cells results in a rapid loss of endocrine BCM, close to >90%[151] and in T2DM, insulin resistance and beta cell dysfunction build up a progressive reduction of BCM, ranging from 25% to 65%[148, 152]. People with either type of diabetes are at high risk of developing a range of complications, such as retinopathy, nephropathy, neuropathy and cardiovascular disease[153], which can endanger their health and survival; consequently, the high costs of care increase the risk of catastrophic medical expenses[154].

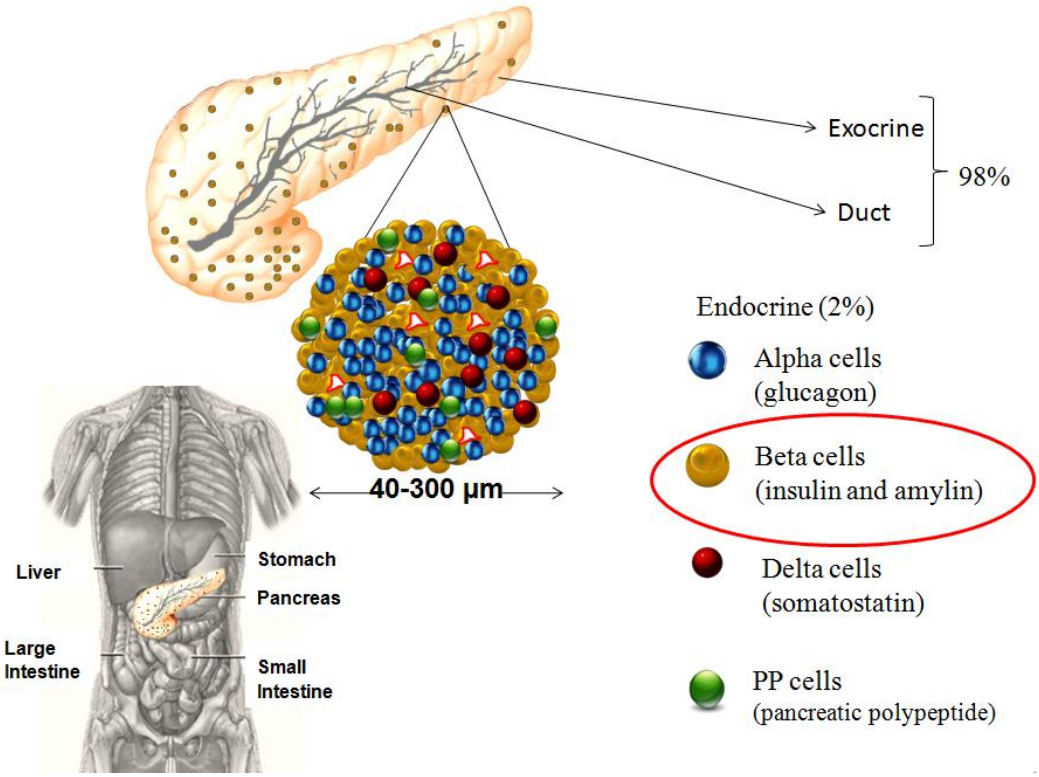

Figure 4. Schematic representation of the location of the human pancreas, Islets of Langerhans and its composition[146, 155].

1.8.1 Beta cell imaging (BCI)

As discussed earlier, functional loss of BCM is associated with both T1DM and T2DM[156]. At present, most information on human BCM during the progress of DM is obtained from post mortem pancreatic biopsy studies, "as a golden standard." *In vivo* biopsies of the pancreas for determination of BCM in either healthy or diabetic patients are associated with complications and therefore unacceptable in clinical studies[157]. The other functional clinical tests such as insulin/C-peptide concentration in the blood as a response to a stimuli, does not reflect on BCM, but rather BCF. Production of insulin in individual beta cells can increase significantly to compensate for the decreased total BCM. Consequently, we lack reliable, reproducible data on the actual progress in BCM during progress of T1DM and T2DM even at group levels. Importantly, we currently lack the tools to follow the fate of BCM longitudinally over time in individual subjects[158].

In T1DM, BCM and its function proportionally decline quite rapidly with the onset of hyperglycemia[159], and in T2DM, diagnosis is sometimes not possible until several years after its onset[160]. Therefore, there is a real need for an accurate and noninvasive *in vivo* imaging technique to study the dynamic changes of BCM at onset and progression of the disease to be able to diagnose early stages of diabetes or at high risk of its development, as well as to

monitor the efficacy of new drugs or stem cell therapy or islet transplantation. An attractive approach to determine BCM *in vivo* is PET, which can detect very low concentrations in subpicomolar range[27] of the radioligand in the target tissue, with high sensitivity. However, several challenges have to be met before developing a PET radioligand for detecting BCM, which is discussed later. The ideal radioligand and the target for BCI have not been found yet. Several ^{11}C and ^{18}F labelled PET radioligands, aiming at three different molecular targets, such as [^{11}C]DTBZ[161] and [^{18}F]fluoropropyl (FP)-DTBZ (targets VMAT2)[162, 163], [^{68}Ga]exendin-4 (targets GLP-1R)[164] and [^{11}C]5-HTP (targets serotonin biosynthesis)[165] have undergone initial clinical validation, but none of them could fulfil all criteria for a 'perfect' BCI agent. An important argument against the use of PET radioligands in endogenous BCM imaging is striking the scientific area, where several theoretical[166], technical and biological limitations are discussed to determine if the sensitivity and specificity are good enough to detect subtle changes of BCM over time[167, 168]. However, PET imaging could be very fruitful to monitor efficacy of glucose lowering drugs for treating T2DM, islets transplantation efficiency and graft survival for treating T1DM patients and thereby, optimise islet transplantation procedures and detect postoperative complications.

In this thesis, three different molecular targets have been explored by using three novel ^{18}F and ^{11}C-labelled radioligands, [^{18}F]FE-DTBZ-d4 (targets VMAT2, Paper **I**), [^{11}C]AZ12504948 (targets glucokinase, Paper **II**) and [^{11}C]AZ compound X (targets GPR44, Paper **III**), for visualising native BCM in the pancreas by PET.

1.9 ALZHEIMER'S DISEASE (AD)

Alzheimer's disease (AD) is a chronic, progressive neurodegenerative disorder and is one of the most common causes of dementia[169], which gradually worsens with the lapse of time in middle or late life. Death occurs, on average, nine years after diagnosis[170]; nevertheless, the onset of the pathological processes occurs probably years prior to the onset of cognitive symptoms[132]. The amyloid hypothesis states that aggregated amyloid-beta (Aβ) peptides have a major role in the development of AD[171, 172]; therefore, *in vivo* imaging of Aβ plaques may be beneficial for the diagnosis, staging and treatment of AD. Over the last decade, the development of amyloid-specific PET radioligands has proved successful for distinguishing between AD and healthy controls. Most radioligands used for Aβ plaque imaging are derived from dyes, such as Congo red (CR) and thioflavin-T (Th-T), which have been used for fluorescent staining of Aβ plaques in postmortem AD brain sections [173, 174]. Two analogues of Th-T; [^{11}C]PIB[175,176] and [^{11}C]AZD2184[177,178] have been used for clinical trials in AD

patients. However, due to short half-life of ^{11}C, alternative ^{18}F-labelled ligands with longer half-lives have undergone clinical trials such as a PIB derivative [^{18}F]flutemetamol (3-[^{18}F]F-PIB),[179,180] AZD2184 derivative [^{18}F]AZD4694,[181] pegylated stilbene and styrylpyridine derivatives, [^{18}F]florbetaben (BAY 94-9172)[182-184] and [^{18}F]florbetapir (AV-45),[184,185] respectively. At present, medications used for treating moderate to severe AD can provide temporary relief from symptoms but no outcome with a strong disease-modifying effect.[186,187] Inhibition of the Aβ peptides formation, thus, emerged as a potential therapeutic approach. To identify BBB, penetrable small molecule drugs such as small peptides that interfere with Aβ peptide interactions, which are expected to prevent and/or cure these diseases, appear attractive. In this thesis, three small 12-mer D-enantiomeric peptides, specific to amyloid plaques ($A\beta_{1-42}$) peptides of AD, were selected to observe the BBB penetration properties for diagnosis and potential therapy for AD.

2 AIMS

The overall aim of the thesis was to develop novel fluorine-18 and carbon-11 labelled PET radioligands for two different important molecular targets: beta cell mass (BCM) for imaging diabetes related health problems and amyloid plaques for imaging Alzheimer's disease (AD).

The specific aims of the thesis were as follows:

1. Development of novel radioligands for visualising endogenous BCM with the following sub-aims:
   a. Radiolabelling of [^{18}F]FE-DTBZ-d4 (targets VMAT2), using fluorine-18 for imaging beta cells by PET and to compare its *in vitro* and *in vivo* binding characteristics with the non-deuterated analogue [^{18}F]FE-DTBZ.
   b. Radiolabelling of [^{11}C]AZ12504948 (targets glucokinase), using carbon-11 for visualising both liver and pancreatic beta cells by PET, as well as to evaluate *in vitro* and *in vivo* characteristics.
   c. Radiolabelling of a ligand targeting GPR44, AZ compound X, using carbon-11 and tritium for beta cell imaging by PET and to evaluate *in vitro* binding using autoradiography in human and rat pancreatic tissue slices.

2. Radiolabelling and *in vitro* evaluation of ^{18}F-labelled D-peptides for visualising amyloid (Aβ) plaques in human brain tissue slices by autoradiography.

3 MATERIALS AND METHODS

A brief summary of the general experiments and methods used during this thesis work are described in this section. However, for the complete experimental details, the reader is referred to the copies of the full papers and manuscripts that follow.

3.1 RADIOCHEMISTRY

Both radionuclides carbon-11and fluorine-18 were produced from a GE PETtrace cyclotron (GE Uppsala, Sweden) using 16.4 MeV protons. All the gases used for positron emitting isotope production were purchased from AGA Gas AB (Sundbyberg, Sweden).

3.1.1 Production of [^{11}C]methyl iodide ([^{11}C]CH_3I)

Carbon-11 was produced by proton bombardment of nitrogen gas via the $^{14}N(p,\alpha)^{11}C$ nuclear reaction. The primary precursor [^{11}C]CH_4 was produced from the mixture of target gas in nitrogen (N_2) with 10% hydrogen (H_2) of scientific grade purity (99.9999%). Throughout this thesis, [^{11}C]CH_4 was further converted to the secondary precursors, [^{11}C]CH_3I and [^{11}C]CH_3OTf using an online procedure. An aluminium target (78 mL) body was used with Havar foils (25 μm), where the target body was cooled using water and the foil using helium (He), respectively. The gas mixture was purified using gas purifier (All Pure^{TM} Alltech) prior to entering the target body to remove any traces of stable carbon-12.

[^{11}C]CH_3I, was produced from [^{11}C]CH_4 following previously published method[67]. In short, [^{11}C]CH_4 was transferred from the cyclotron to the dedicated methyl iodide synthesiser (methane system, DMA, Stockholm, Sweden) by Helium pressure (500 mL/min) and passed through a phosphorous pentoxide (P_2O_5) trap to remove traces of ammonia and water produced during the nuclear reaction. After passing through P_2O_5 trap, [^{11}C]CH_4 was trapped in a Porapak Q trap with liquid N_2, which was purged with He to remove any unreacted target gases. Following collection, [^{11}C]CH_4 was released from the Porapak Q trap by heating with pressurised air into a recirculation system via He flow. The recirculation system consisted of a micro diaphragm gas pump (NMP830KVDC, KNF Neuberger, and Freiburg, Germany), quartz tube containing iodine and ascarite, three ovens, as well as a Porapak Q trap. The [^{11}C]CH_4 was first pumped to the quartz tube, where it was mixed with vapour of iodine crystals at 60°C (1st oven), and then the radical reaction occurred in the reaction chamber at 720°C (2nd oven) to produce [^{11}C]CH_3I. Produced [^{11}C]CH_3I was trapped at RT to Porapak Q

trap, and the excess amounts of iodine and by-product hydroiodic acid (HI) were trapped on ascarite (sodium hydroxide coated silica trap). The unreacted [^{11}C]CH_4 was recirculated for 3–4 min to reach the maximum amount of [^{11}C]CH_3I in the Porapak Q trap (Figure 5). [^{11}C]CH_3I was further released from the Q trap by heating the homemade oven (3rd Oven) at 180°C; subsequently, it was trapped in a suitable solvent or reaction mixture where the radiosynthesis i.e. methylation reaction, HPLC purification and formulation took place. The preparation of [^{11}C]CH_3I was ready for use within 10–11 min from the end of radionuclide production (Figure 5).

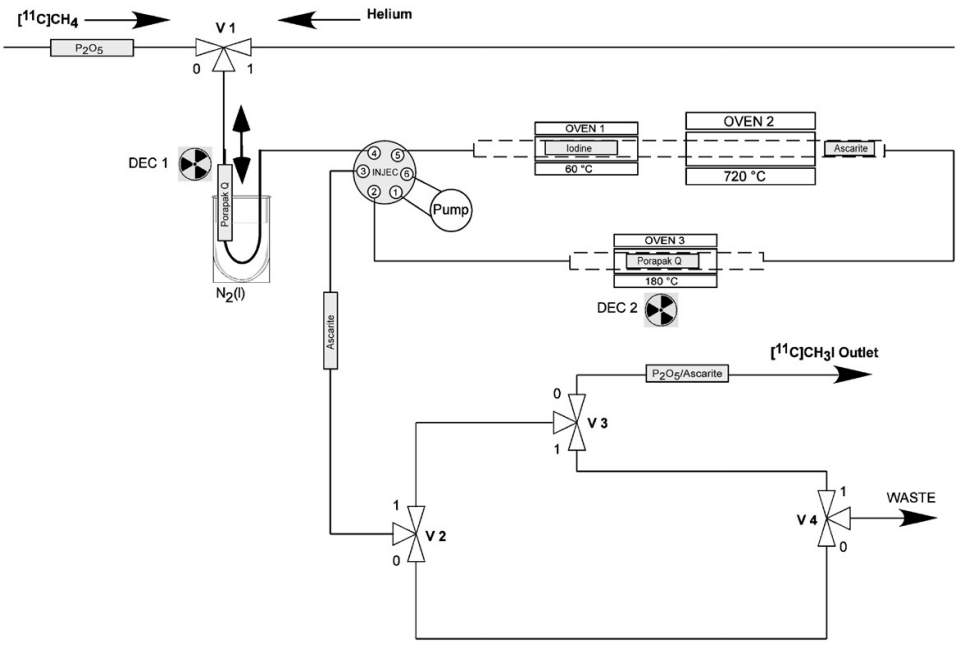

Figure 5. Flow chart for production of [^{11}C]CH_3I from in-target produced [^{11}C]CH_4 via gas phase iodination[67].

3.1.2 Production of [^{11}C]methyl triflate ([^{11}C]CH_3OTf)

Carbon-11 labelled [^{11}C]CH_3OTf was produced from [^{11}C]CH_3I, following previously described method.[73,188] Produced [^{11}C]CH_3I was passed in a stream of He gas through a soda-glass column (i.d: 3.7 mm; length 150 mm; oven temperature 165°C) containing silver triflate-impregnated graphitized carbon. The formed [^{11}C]CH_3OTf was trapped in appropriate solvent containing precursor material.

3.1.3 Radiosynthesis, purification and formulation of ^{11}C-radiopharmaceuticals

The methylation reaction was performed in a fully automated custom built synthesis module (Scansys, Copenhagen, Denmark), where a PC programme is developed for the

control and programming of the system. The operator gets running information during the synthesis. During the entire process, the radioactivity was monitored using GM radio detectors. The reagents and solution used during the synthesis were placed in a clean air atmosphere. Radiosynthesis, purification and formulation of the final product took place under HEPA filtered air.

Radioligand [^{11}C]AZ12504948 (Paper **II**) and [^{11}C]AZ compound X (Paper **III**) were synthesised by *O*-methylation and *S*-methylation, respectively, using [^{11}C]CH_3I as methylating agent in one step. [^{11}C]AZ12504948 was obtained by trapping [^{11}C]CH_3I at room temperature in a reaction vessel containing the precursor AZ12555620 (1.0 mg–1.6 mg, 2.16 μmol–3.45 μmol) and freshly powdered solid potassium hydroxide (KOH) (10–13 mg, 178 μmol–232 μmol) in dimethylsulfoxide (DMSO) (300 μL). After end of [^{11}C]CH_3I trapping, the reaction mixture was diluted with sterile water (500 μL) before injecting to the built-in high performance liquid chromatography (HPLC) system for purification of the labelled compound.

[^{11}C]AZ Compound X was synthesised by trapping [^{11}C]CH_3I at room temperature in a reaction vessel containing the precursor (1.0 mg–2.0 mg, 2.48 μmol–4.95 μmol) in dimethylformamide (DMF) (300 μL). After end of [^{11}C]CH_3I trapping, the reaction mixture was heated at 70°C for 5 minutes. The reaction mixture was diluted with sterile water (500 μL) before injecting to the built-in HPLC system for the purification of the labelled compound.

The chromatographic process was monitored in real time by means of UV detector and GM radio detector; furthermore, the HPLC column was scanned continuously by means of an extra GM radio-detector. After collecting the pure fraction of the corresponding radioligand, evaporation of the mobile phase was performed continuously online by stream of He using a carburetor. The labelled product was accumulated in the carburetor spiral, which was heated to moderate temperature (80°C), while the mobile phase was evaporated off. The HPLC system consisted of a pump (Gilson 304), an automated sample injector (Gilson 234 autoinjector) and an ACE column (RP C18, 10 × 250 mm, and 5 μm). The formulation of the final product was accomplished by flushing the spiral with sterile phosphate buffer saline (PBS) and followed by filtration through a sterile filter (0.22 μm; Millipore, Sweden) into a sterile vial to get pyrogen free solution before applications. Self-cleaning routines of the auto-sampler syringe, HPLC system, evaporator and tubing were executed, before and after the synthesis. All the running information during the synthesis was printed out after the completion of the synthesis.

3.1.4 Production of fluorine-18

Fluorine-18 fluoride, [^{18}F]F$^-$, was produced from bombardment of ^{18}O-enriched water ([^{18}O]H_2O), using the ^{18}O(p, n)^{18}F nuclear reaction from high pressurised silver target[189]. Produced [^{18}F]F$^-$ was transferred to the dedicated hot cell with He pressure and isolated from [^{18}O]H_2O to a pre-conditioned [i) 10 mL 0.5 M K_2CO_3 solution ii) 15 mL water (18 MΩ)] SepPak QMA light anion exchange cartridge (Waters). Trapped [^{18}F]F$^-$ was eluted from the QMA cartridge with QMA eluent (1.5–2.0 mL), which consisted of a mixture of K_2CO_3, Kryptofix$_{2.2.2.}$ (4,7,13,16,21,24-hexaoxa-1,10-diazabicyclo-[8.8.8.]hexacosane-$K_{2.2.2.}$) in water and acetonitrile, via N_2 flow to a reaction vessel[190]. The QMA eluent was evaporated to dryness at 160°C under continuous N_2 flow to form a dry complex of [^{18}F]F$^-$ /K_2CO_3/$K_{2.2.2.}$, and the residue was cooled to RT. The preparation of dry complex, [^{18}F]F$^-$ /K_2CO_3/$K_{2.2.2.}$, was ready to use within 20–21 min after the end of radionuclide production (Figure 6).

3.1.5 Radiosynthesis, purification and formulation of ^{18}F-radiopharmaceuticals

The ^{18}F-radioligands synthesis (Papers **I** and **IV**) including HPLC purification, SPE isolation, as well as formulation of the final product took place in a semi-automatic ^{18}F-synthesis module (FIA-1 DMA, Figure 6). All valves, temperatures (R1 and R2) and radio-detector output were possible to control or monitor using a touch screen. Flow of N_2 gas was controlled by a needle valve and was followed by the flow metre, which was situated outside and inside of the hot cell, respectively.

In paper **I**, precursor, 1-bromoethyl-2-tosylate-d4 (BrEtOTs-d4, 15 µL) was dissolved in aprotic polar solvent *o*-DCB (700 µL) and mixed with dry complex of fluoride, [^{18}F]F$^-$ /K_2CO_3/$K_{2.2.2}$ to synthesise the prosthetic group [^{18}F]fluoroethylbromide-d4, ([^{18}F]FEtBr-d4). The reaction mixture (RM) was heated at 160°C for 10 min to produce crude [^{18}F]FEtBr-d4, which was purified by fractional distillation and collected in a second vial containing desmethyl-DTBZ precursor (2.0–2.5 mg, 6.55–8.19 µmol), sodium hydroxide (15 µL, 5M) in DMF (500 µL). The vial was placed in the 2nd reactor (R2 in Figure 6), and the RM was heated at 110°C for 5 min to produce crude [^{18}F]FE-DTBZ-d4.

In paper **IV**, prosthetic group *N*-succinimidyl-*4*-[^{18}F]fluorobenzoate, [^{18}F]SFB, was synthesised following the previously described method after modifications[191, 192]. The precursor 4-trimethylammoniumbenzoate trifluoromethanesulfonate (**1**) (5.0 mg, 20 mmol) in anhydrous MeCN (1 mL) was added to the dry [^{18}F]F$^-$/K_2CO_3/$K_{2.2.2}$ complex, and the RM was heated at 90°C for 10 min to produce ethyl-*4*-[^{18}F]fluorobenzoate ([^{18}F]**2**), which was

used for the next reaction without further purification. [^{18}F]**2** was treated with tetrabutylammonium hydroxide (TBAH) (13 µL, 1 M in water) in 0.2 mL MeCN by heating at 120°C for 3 min to produce 4-[^{18}F]fluorobenzoic acid salt ([^{18}F]**3**). The mixture was dried azeotropically using MeCN (1 mL) at 160°C under continuous N_2 flow to remove excess water from the addition of the aqueous solution of TBAH. The RM was cooled to 40°C, and a solution of the reagent *N*,*N*,*N*,*N*-tetramethyl-O-(*N*-succinimidyl)uronium hexafluoro-phosphate (HSTU) (12 mg, 33 mmol) in MeCN (1 mL) was added to [^{18}F]**3** and heated at 90°C for 5 min to produce [^{18}F]SFB, which was purified by semi-preparative HPLC followed by SPE isolation (HLB 60 mg) before use in the next step. Pure [^{18}F]SFB was eluted with MeCN (~800 µL) from the SPE and used for the radiolabelling of [^{18}F]D-peptides, ([^{18}F]ACI-87-F, [^{18}F]ACI-88-F and [^{18}F]ACI-89-F). In a solution of [^{18}F]SFB (200 µL ~ 900 MBq) in MeCN, precursor peptides (1.2 mg) in borate buffer (0.5M, pH 8.8; 150 µL) solution were dissolved and kept at RT for 10 min to produce crude [^{18}F]D-peptides. Three [^{18}F]D-peptides were purified using analytical HPLC column (RP C18, 3.9×300 mm, 10 µm, Waters). The radiosynthesis and purification of [^{18}F]D-peptides were performed in another hot cell, which is not included in Figure 6.

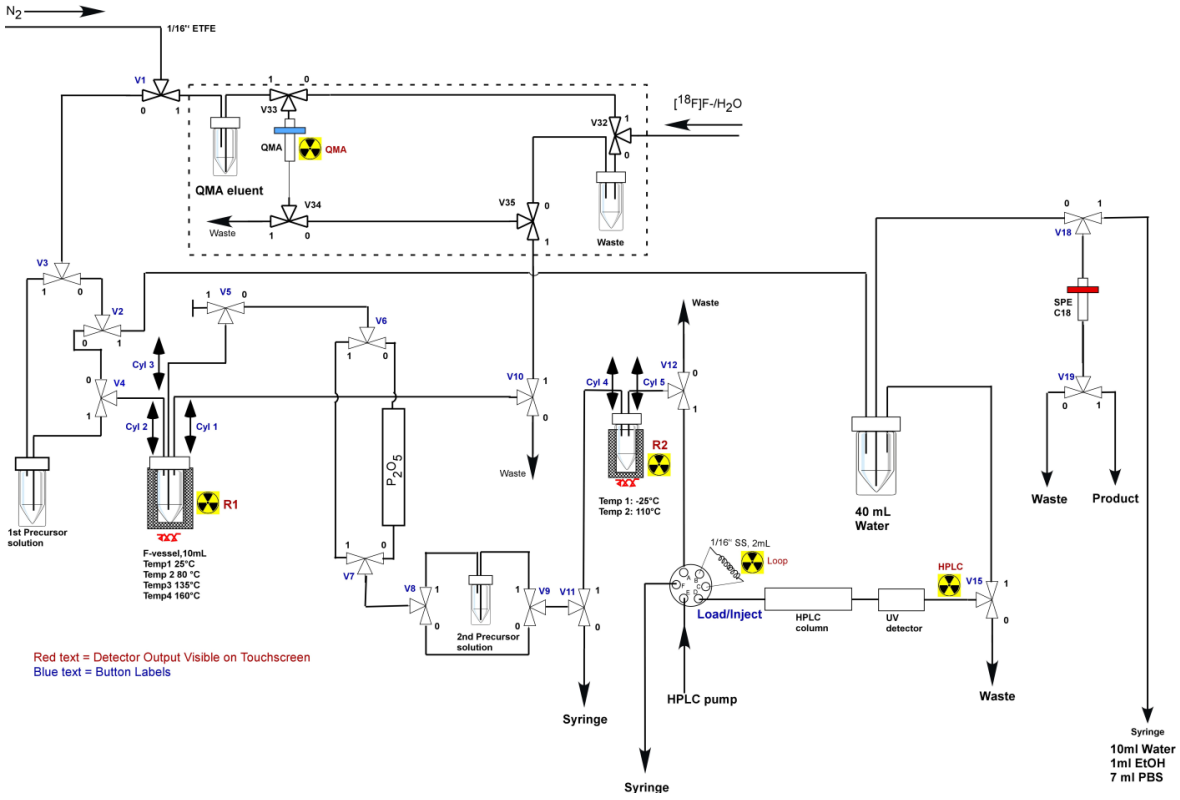

Figure 6. Flow chart of production of both one step (only one reactor R1 is used) and two steps (both reactors R1 & R2 are used) fluorine-18 labelled radiopharmaceuticals, purification and formulation.

After the reaction, the crude reaction mixture was cooled to RT and was injected manually to the built-in HPLC purification system (Figure 6). The HPLC system consisted of a μ-Bondapak column (RP C18, 7.8×300 mm, 10 μm, Waters) and a UV detector in series with a GM tube. The pure fraction of the corresponding ^{18}F-radioligand was collected in a bottle containing water (40–50 mL) for dilution, which was continuously passed through a pre-conditioned SPE (tC18 plus) cartridge [i) ethanol (10 mL) and ii) sterile water (10 mL)] by stream of N_2 gas for isolation. SPE was washed by water (10 mL) using the manual syringe which was positioned outside of the hot cell. The formulation of the final product was accomplished by flushing the SPE with ethanol (<10%) and sterile PBS solution and collected in a sterile vial (Figure 6). All formulated ^{18}F-labelled radioligands were filtered through a sterile filter (0.22 μm; Millipore, Sweden) into a sterile vial to get pyrogen free solution before applications. The aseptic work was performed in a laminar air flow workstation (LAFW).

3.2 QUALITY CONTROL OF ^{11}C AND ^{18}F LABELLED RADIOPHARMACEUTICALS

The radiochemical purity, identity and stability of ^{11}C and ^{18}F labelled radiopharmaceuticals were identified using analytical HPLC. The HPLC system consisted of RP analytical column, Merck-Hitatchi L-7100 Pump, L-7400 UV detector in series with a radioactivity detector (β-flow; Beckman, Fullerton, CA) for radioactivity detection. The identity of ^{11}C and ^{18}F labelled radiopharmaceutical(s) was confirmed by co-injection of the radiopharmaceutical(s) with its unlabelled reference standard, where the retention time of the radiopharmaceutical(s) was compared to that of the unlabelled reference standard. The stability of the radiopharmaceutical(s) was tested at different time intervals: 30, 60, 90, 120 minutes after end of radiosynthesis.

3.3 SPECIFIC RADIOACTIVITY (SRA) DETERMINATION

The specific radioactivity (SRA) of all radiopharmaceutical(s) was measured using analytical HPLC system from Merck-Hitachi with D-6200A pump, L-4000 UV detector and D-6000 interface. SRA was calibrated for UV absorbance response per mass of ligand and calculated as the radioactivity of the radioligand (GBq) divided by the amount of associated carrier substance (μmol). Each sample (radioligand after decay) was analysed three times and compared to a reference standard (known concentration) which was also analysed three times, by taking same amount of the sample by the auto-sampler of the HPLC system.

3.4 LIQUID CHROMATOGRAPHY-MASS SPECTROMETRY (LC-MS/MS) ANALYSIS

The structure of ^{11}C and ^{18}F radiopharmaceuticals were further confirmed by comparing LC and MS fragmentation pattern of the reference standards and that of the carrier of the corresponding nonradioactive compounds. LC-MS/MS analysis was performed using a Waters Acquity™ ultra performance LC system connected with a Micromass premier™ Quadrupole time of flight (TOF) mass spectrometer (Waters, Milford, MA, USA). LC was performed using a Waters Acquity UPLC™ BEH column (C18, 2.1 × 50 mm, 1.7 µm particle size) kept at 50°C. The mobile phase consisted of 0.1% formic acid in water (A) and 0.1% formic acid in ACN (B). Samples were analysed using a linear gradient at a flow rate of 0.5 mL/min. The MS was operated in positive electrospray ionization (+ESI) mode, with the following settings: capillary voltage 3.0 kV; cone voltage 35 V; source temperature 100°C; dissolvation temperature 400°C and collision energy 20 eV. The formulated product, ^{11}C and ^{18}F radiopharmaceuticals, was analysed after radioactive decay without further dilution.

3.5 *IN VITRO* AUTORADIOGRAPHY

Biopsies from human pancreas and liver of healthy subjects and type 2 diabetic (T2D) subjects were collected from deceased human donors (Paper **II-III**). The use of human tissue was approved by the Uppsala Ethical Review Board (Dnr 2015-401; # 2011/473, #Ups 02-577) and tissues obtained from Uppsala Biobank. The biopsies were frozen to -80°C and processed into 20 µm slices. Slides were kept at -20°C until use.

AD human brain (Paper **IV**) was obtained from the Alzheimer Brain Bank of the University of Szeged, Hungary. The age matched control human brain was obtained from the Institute for Forensic Medicine, Semmelweis University, Budapest, Hungary. Brains had been removed during a forensic autopsy and were handled in a manner similar to that previously described[193, 194]. Fresh frozen whole hemisphere brain slices (100 µm) was prepared. Ethical permissions for the study were obtained from the relevant university ethical boards. Slides were kept at -20°C until use.

In paper **II**, to study radioligand binding properties of different tissues, pancreas [healthy (*n=1*), T2D (*n=2*)] and liver [healthy (*n=1*)], slices were incubated in different concentration (0.05-1.0 nM) of the radioligand, [^{11}C]AZ12504948, in 50 mM TRIS HCl containing 5 mM D-(+)-glucose (Sigma-Aldrich, St Louis, MO, USA) and 0.4 mg/mL β-

cyclodextrin (Kleptose HPB, original formulation 300 mg/mL, Apoteket, Umeå, Sweden) for 40 minutes at RT. Non-displaceable binding was assessed by adding excess amount of (11-13 μM) of unlabelled AZ12504948. Tissue slices were washed twice for two minutes in 50 mM TRIS HCl containing 5 mM D-(+)-glucose at RT to remove excess tracer, followed by a brief wash in distilled water and then dried for 5 min on a hot-plate (37°C). The slices were then exposed to a phosphor-imager screen (Amersham Biosciences, Uppsala, Sweden) for 4-6 hours, scanned using a Phosphorimager SI (Molecular Dynamics, Sunnyvale, CA, USA) and analysed using ImageQuant (Molecular Dynamics, Sunnyvale, CA, USA). The affinity for the specific binding was expressed as the dissociation constant K_d, determined by GraphPad Prism 5 (San Diego, CA, USA).

In paper **III**, sections of pancreas from non-diabetic (*n=6)* and T2DM (*n=6*) as well as from Sprague Dawley rats (*n=4*) for ARG experiments using the PET ligand [^{11}C]AZ compound X, were pre-incubated in 100 mL 50 mM PBS (pH 7.4) for 10 minutes. Then, radioactivity corresponding to 1 nM [^{11}C]AZ Compound X (*n=3*) was added, and sections were incubated with the radioligand for 30 min at RT. Non-displaceable binding was assessed in a separate assay, by co-incubation with 20 μM of the GPR44 antagonist AZ Compound Y. Autoradiography (ARG) experiments using tritiated ligand, [^{3}H]AZ Compound X, were performed by following similar procedure as described for [^{11}C]AZ Compound X, except all sections were (healthy, *n=3* and rats *n=3*) incubated with 1 nM [^{3}H]AZ Compound X at RT for 3 hours. Following incubation, tissue sections were washed 3 times for 2 minutes in 50 mM PBS at 4°C. The sections were dried and exposed to phosphor-imager screen for 40 minutes with [^{11}C]AZ Compound X and 90 hours with [^{3}H]AZ Compound X.

In paper **IV**, ARG was performed on fresh frozen whole hemisphere brain slices. The incubation buffer consisted of TRIS HCl (50 mM) including NaCl (120 mM), KCl (5 mM), $CaCl_2$ (2 mM) and $MgCl_2$ (1 mM), as well as 10 μM pargylin and 0.3% bovine serum albumine, pH 7.4. The brain slices were incubated with the buffer at radioligand concentration of 0.02 MBq/mL with [^{18}F]-peptides for 90 min, at RT. The measurements were done in duplicates. The slices were then rinsed with a buffer consisting of TRIS HCl (50 mM), three times for 5 min each at 4°C; followed by dipping in ice cold distilled water.

The slices (Papers **III-IV**) were scanned using a Cyclone Plus Phosphor imager (Perkin Elmer) at 600 dpi in case of [^{11}C]AZ Compound X and [^{18}F]peptides, as well as Fujifilm BAS-5000 phosphor imager (Fujifilm, Tokyo, Japan) in case of [^{3}H]AZ Compound X. The images were analysed using ImageJ (NIH). Specific binding was defined by subtracting non-displaceable binding from total binding.

3.6 HOMOGENATE TISSUE SATURATION BINDING

Isolated endocrine and exocrine tissues from human pancreas[195] were homogenised by using a polytron tissue homogeniser (Polytron® PT 3000, Kinematica AG, Littau, Switzerland) and incubated in TRIS [tris(hydroxymethyl)aminomethane] (50 mM) solution. The tissue homogenates (0.5–6 mg/mL) were incubated in 1 mL TRIS (pH 7.4) with different concentrations of specific ^{11}C- or ^{18}F-radioligand around an expected K_d. Aliquots of the homogenates were stored at -80^{o}C until used. All homogenised endocrine and exocrine samples were incubated separately for 30 to 60 min at RT with radioactivity and then moved onto a Brandel 1.2 μm Whatman filter (pre-treated with 0.05% polyethylenimine or TRIS) by M-48 cell harvester (Brandel, Gaithersburg, MD, USA). The filter was washed four times with 3 mL TRIS (RT) and measured in a well-counter (Uppsala Imanet AB, GE Healthcare, Sweden). Tissue samples and references were prepared in triplicates and filter binding controls in duplicates. Non-displaceable binding was accessed by adding unlabelled cold ligand in high concentration (10–20 μM) to the incubation buffer. The specific binding was calculated by subtracting the non-specific binding from the total binding, and the endocrine-to-exocrine binding ratio was calculated. Tissue protein content (mg protein/sample) was assessed by a BioRad Protein Assay (BioRad, Hercules, CA, USA), and absorbance was measured with an EL808 microplate reader (BioTek, Winooski, VT, USA). The Binding Potential (BP), (B_{max}/K_d), was determined by non-linear regression (Paper **I**).

3.7 PET/CT IN PIG AND NONHUMAN PRIMATE (NHP)

Swedish Landrace piglets were used in this thesis work and were housed under the proper lab conditions. All procedures were approved by the local ethical committee for animal experimentation (Uppsala, Sweden; ethical permit Dnr C 245/8) and performed in accordance with local institutions and Swedish national rules and regulations. Piglets were anesthetised by using ketamine and morphine and they were intubated and placed on a ventilator. The anaesthesia was maintained by 2.5% sevofluran. Normoglycemia was confirmed by determining blood glucose content (4.4 to 7.6 mM) using an i-STAT analyser (CG8+cartridges, Abbot Point-of-Care, Inc, Princeton, NJ, USA). Animals were administered 5.9–20.6 MBq/Kg of the radioligand intravenously (baseline scan, *n=3*), and the blocking study (*n=2*) was performed by co-administration with 1.5 mg/kg unlabelled ligand formulated in a mixture of sterile ethanol (30%) in propylene glycol and sterile PBS (3:5) to study the specific binding. The pharmacological effect was analysed by comparing decrease

in plasma glucose levels before and 90 min after unlabelled ligand administration. The biodistribution as well as kinetics of the radioligand were studied by a Discovery ST PET/CT scanner (GE, Milwaukee, WI, USA) for 90 min with a dynamic sequence of (30 sec frames x 4, 1 min frames x 3, 3 min frames x 5, 5 min frames x 14). The CT scans were acquired for attenuation correction. Arterial (Paper **I**) and venous (Paper **II**) blood samples were acquired throughout the study and centrifuged at 3500 rpm for 5 minutes to separate the plasma. Both whole blood and plasma were measured for radioactivity using the well counter.

Cynomolgus monkeys (*Macaca fascicularis*), housed in the Astrid Fagraeus laboratory, Karolinska Institutet, Solna, Sweden. The experiment with the monkey was approved (N 399/08) by the Animal Ethics Committee of the Swedish Animal Welfare Agency and was performed according to the Guide for the Care and Use of Laboratory Animals[196]. One cynomolgus monkey (male, 5.4 kg) was used in this thesis (Paper **II**); the monkey handling, anaesthesia and PET/CT procedure were under the control of research nurses. The anaesthesia was induced by intramuscular injection of ketamine hydrochloride and maintained by intravenous infusion of ketamine hydrochloride and xylazine hydrochloride. The body of the monkey was immobilised using a vacuum pad. Blood glucose content was assessed by using an i-STAT analyser (CG8+cartridges, Abbot Point-of-Care, Inc, Princeton, NJ, USA). The monkey was positioned in order to view the abdomen in the field of view (FOV). The whole body PET measurement was performed for 120 min (3-min frame x 3, 4-min frame x 3, 5-min frame x 3, 6-min frame x 14) in a PET/CT scanner (Siemens Biograph 64). Baseline and blocking studies were accomplished by administration of 34 and 37 MBq/kg of the radioligand, respectively. The blocking study was performed by co-administration with 0.5 mg/kg unlabelled ligand formulated in a mixture of sterile ethanol (30%) in propylene glycol and sterile PBS (3:5).

Tissue uptake and kinetics for both pig and NHP were obtained by delineating VOIs on partially summed PET images assisted by CT morphology. All image analysis was performed with the PMOD software (PMOD Technologies Ltd, Zürich, Switzerland). Measurements of the uptake were analysed by using standardised uptake value (SUV), which is the regional tissue radioactivity concentration normalised for the injected dose and body weight of the subject.

$$\%\mathrm{SUV} = \frac{\text{tissue radioactivity concentration (kBq/cc)}}{\text{injected radioactivity (kBq)}} \times \text{body weight (g)} \times 100$$

4 RESULTS AND DISCUSSION

4.1 RADIOLABELLING AND BIOLOGICAL EVALUATION OF DEUTERATED [^{18}F]FE-DTBZ-D4 (PAPER I)

Dihydrotetrabenazine (DTBZ) is highly specific for the vesicular monoamine transporter type 2 (VMAT2), and VMAT2 is co-localised with insulin in islets but is not detectable in exocrine pancreas[197]. [^{11}C]-(+)-DTBZ has been shown to be a BCM biomarker with a potential to distinguish between healthy and diabetic subjects longitudinally, however, with some difficulties[161]. Development of ^{18}F-labelled DTBZ derivative such as [^{18}F]fluoroalkyl-DTBZ[198-200] and [^{18}F]fluoroepoxide-DTBZ[201] appeared in order to get improved version of [^{11}C]DTBZ as BCM biomarker, since ^{18}F has longer half-life and higher electronegativity compared to ^{11}C. The radioligand, [^{18}F]FE-DTBZ, was investigated by our group in 2010 as a first attempt for the development of BCM biomarker; at that time, we found that the radioligand was metabolised extensively by *in vivo* defluorination in a large piglet model[202]. In order to improve the *in vivo* stability, deuterated analogue of [^{18}F]FE-DTBZ was designed, which could improve the VMAT2 uptake in BCM as well as in central nervous system (CNS). The *in vitro* and *in vivo* results of deuterated FE-DTBZ-d4 were compared retrospectively to that of the non-deuterated FE-DTBZ radioligand.

[^{18}F]FE-DTBZ-d4 was synthesised in two steps via indirect fluorination strategy following the previously described method, with slight modifications[203] (Scheme 1). In the first step, the prosthetic group [^{18}F]FEtBr-d4 was synthesised by aliphatic nucleophilic substitution reaction via S_N2 mechanism, where the tosylate (-OTs) leaving group of the precursor BrEtOTs-d4 was substituted with [^{18}F]fluoride and formed [^{18}F]FEtBr-d4. In the second step, the final ^{18}F-product [^{18}F]FE-DTBZ-d4, was synthesised via the coupling of the [^{18}F]fluoroethyl-d4 moiety to the 9-*O*-desmethyl-DTBZ precursor. Purification of [^{18}F]FEtBr-d4, was performed by distillation and isolated in good yield. The conversion of the second step i.e. conversion of [^{18}F]FEtBr-d4 to [^{18}F]FE-DTBZ-d4 was >70% based on analytical HPLC analysis. Determination of pH and volume, and visual inspections of the final formulated product were performed before releasing it for the QC analysis. The total time of the radiosynthesis, including purification and formulation, was 100±20 min after the end of ^{18}F-production. [^{18}F]FE-DTBZ-d4 was produced in good and reproducible radiochemical yield; 1.7 to 3.0 GBq of the pure product was obtained from 20 to 25 min of proton bombardment with beam current of 35 μA. The radiochemical purity was >98% up to 2 hours after EOS, and QC analysis was performed before releasing the radioligand for applications

such as *in vitro* ARG, homogenate binding and *in vivo* PET/CT studies. The structure of the radioligand was further confirmed by comparing the LC-MS/MS data of both reference standard and carrier of the [^{18}F]FE-DTBZ-d4 (after decay). The retention time of the formulated product and the fragmentation pattern of the parent peak were identical to that of the reference standard. SRA of [^{18}F]FE-DTBZ-d4 was high, with a range of 192–529 GBq/μmol after EOS.

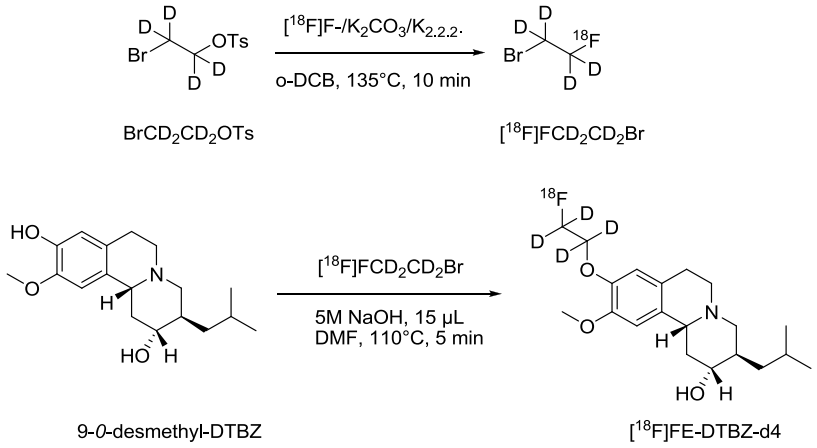

Scheme 1. Synthesis of [^{18}F]FE-DTBZ-d4 using [^{18}F]FEtBr-d4 as alkylating agent in two steps.

The *in vitro* BP ratio of deuterated [^{18}F]FE-DTBZ-d4, in human endocrine and exocrine tissue homogenate was slightly higher than that of the non-deuterated [^{18}F]FE-DTBZ analogue (16 vs 11) i.e. greater tissue discrimination. The *in vivo* PET/CT piglet studies (*n=3*) showed homogeneous uptake of the radioligand in the pancreas with no difference in the head, tail and body of the tissue. The average uptake of the radioligand, expressed in SUV, reached 2.64 shortly after the I.V. administration with a SUV of 1.8 after 90 min, which was comparable to that of the non-deuterated version. Notable accumulation was observed in the liver and spleen with faster washout kinetics than the pancreas. Apart from the excretion through the bile system, excretion through the kidney, bladder and urethra was also observed (Figure 7a). The main goal of the study was achieved by observing reduced bone uptake of the deuterated radioligand *in vivo*, where it showed moderate uptake (SUV 1.4) of radioactivity with no further accumulation (Figure 7b), whereas the bone uptake increased linearly with time for the non-deuterated analogue (SUV of 3.1 at 90 min). However, there was no significant difference observed in specific VMAT2 binding uptake in the pancreas in *in vivo* PET/CT studies, even though more native [^{18}F]FE-DTBZ-d4 was present in blood plasma.

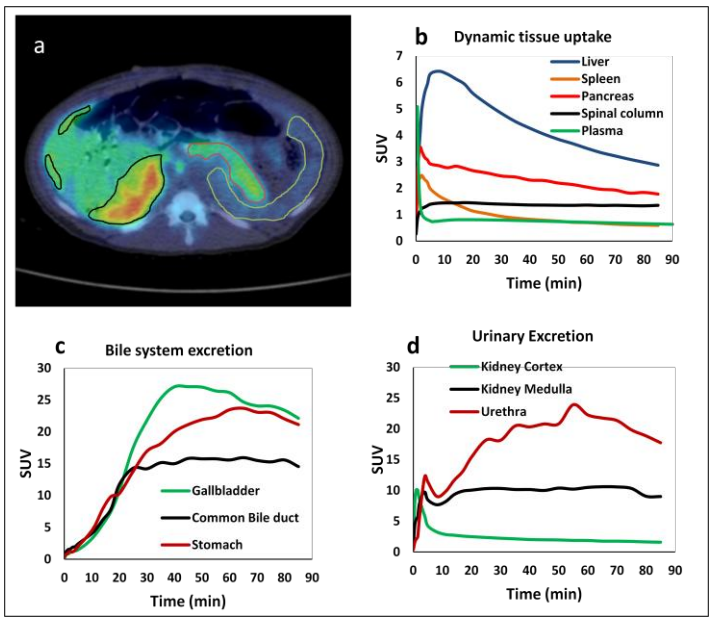

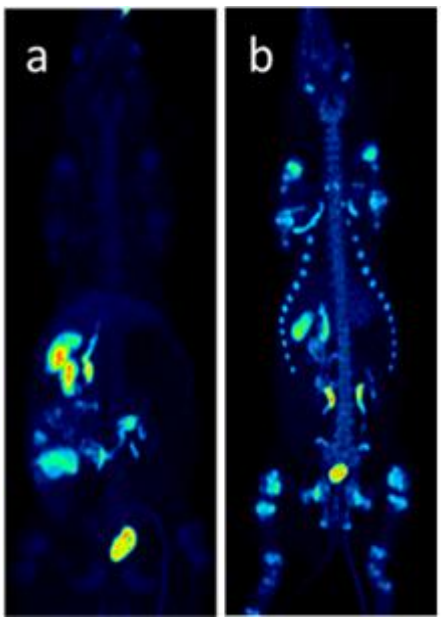

Figure 7a **Figure 7b**

Figure 7. (7a): Delineation of pancreas (red), spleen (green) and parts of the anterior and posterior hepatic segments (black) exemplified on a transaxial PET/CT fusion image (a). The average dynamic uptake of [^{18}F]FE-DTBZ-d4 in pancreas and other abdominal tissues from 4 different piglets (b). Excretion through the biliary system is the fate of a majority of the tracer and its metabolites (c), but there is also elimination of tracer by urine (d). **(7b):** 3D Maximum Intensity Projection (MIP) 90 minutes after administration of (a) [^{18}F]FE-DTBZ-d4, low accumulation in bone structures indicates low levels of free [^{18}F]F$^-$. (b) non-deuterated [^{18}F]FE-DTBZ, high accumulation in bone structures due to higher levels of free [^{18}F]F$^-$. Colours indicate SUV 0 (black) to SUV 30 (white).

4.2 RADIOLABELLING AND BIOLOGICAL EVALUATION OF [^{11}C]AZ12504948 IN PANCREAS AND LIVER (PAPER II)

Glucokinase (GK) is an enzyme predominantly present in the beta cells of the islets of Langerhans in the pancreas[204] and hepatocytes in the liver[205] and as a result, is a potential target for BCM visualisation. GK is regulated by a class of small molecules called glucokinase activators (GKAs). GKAs increase the enzymatic activity of GK upon binding to a hydrophobic pocket, thereby, stabilising the bound state between GK and its substrates[206]. The GKA mechanism of action offers a pharmaceutical target for control of hyperglycemia; therefore, GKAs have been a hot topic in drug development[207, 208].

A novel GKA radioligand, [^{11}C]AZ12504948, was synthesised by *O*-methylation using a combination of methylating agent [^{11}C]CH_3I, base $KOH_{(s)}$ and DMSO as solvent in one step at RT (Scheme 2). The solution of the aliphatic desmethyl precursor, AZ12555620, with freshly powdered KOH in DMSO, needed to be vortex for ten min to ensure formation of the alkoxide anion prior to labelling with [^{11}C]CH_3I. Besides DMSO,

DMF was also used as solvent for the reaction but did not result in the formation of the desired labelled product. Several bases such as sodium hydride (60% in oil), aqueous NaOH (5M and 0.5M), triethylamine, solid powdered K_2CO_3, KOH and NaOH were assessed; however, only $NaOH_{(S)}$ resulted in the desired labelled product. Reaction parameters such as temperature (RT-140°C), reaction time (1–15 min), amount of precursor used (0.2–1.6 mg) were also investigated. Heating the reaction mixture did not improve the yield but started the decomposition of the formed [^{11}C]AZ12504948. It was observed that the radiochemical conversion of [^{11}C]CH_3I to the desired product [^{11}C]AZ12504948 was dependent on the used concentration of the precursor. Further experiments were performed to optimise the RCY by using the identical reaction conditions but with variation in the amount of precursor AZ12555620 used. The RCY varied from 10%–85%, depending on the amount of the precursor (0.2 mg–1.6 mg), and the yield reached maximum when amount of the precursor was >1.0 mg.

The total time of radiosynthesis including purification and formulation of the product was 28–30 min after end of the radionuclide production. The synthesis was highly reproducible, and the conversion of [^{11}C]CH_3I to [^{11}C]AZ12504948 was >90% (based on analytical HPLC). It was possible to produce up to 3000 MBq of pure product from 30 min of proton bombardment, at beam current of 35 μA, for PET studies. The radiochemical purity was >98% up to 2 hours after EOS. The specific radioactivity ranged from 582–2350 GBq/μmol after EOS. The precursor, AZ12555620, had two active sites for alkylation, which potentially could be radiolabelled by ^{11}C-methylation, either at the *N*-position of the secondary amide or at the *O*-position of the aliphatic hydroxyl group. The goal was to label at *O*-position with ^{11}C to get the desired product [^{11}C]AZ12504948 (Scheme 2). The position of the methylation, *O*-alkylation instead of *N*-alkylation, was confirmed by comparing the LC-MS/MS fragmentation of the reference standard and precursor compound.

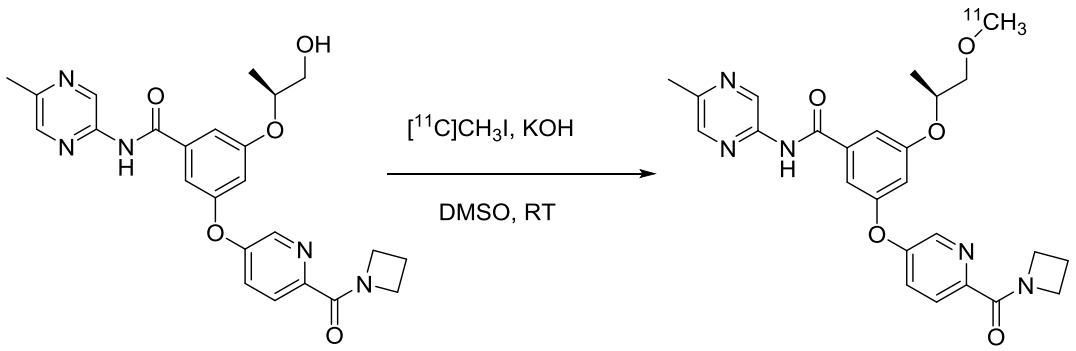

Scheme 2. Radiosynthesis of [^{11}C]AZ12504948 via [^{11}C]CH_3I.

In vitro ARG saturation binding study in human tissues showed around 50% specificity (47.3±4.1%) to liver and low specificity (only 7.8%±3.6%) to pancreas from non-diabetic human donors at sub-nanomolar concentration of [^{11}C]AZ12504948. However, despite the low portion of specific receptor binding in the *in vitro* studies, we decided to perform additional studies using pigs to observe the bio-distribution of [^{11}C]AZ12504948 in baseline condition and the specificity of [^{11}C]AZ12504948 by performing blocking experiments (co-injection of cold ligand, 1.5 mg/kg). During the blocking experiments, pharmacological effect of the cold ligand (GKA), AZ12504948, was followed by measuring the blood glucose concentration, which decreased from 5.2 to 3.6 mM (measurement 1) and from 4.0 to 2.7 mM (measurement 2). The baseline studies demonstrated moderate uptake in the pancreas and slightly higher uptake in the liver following similar kinetics. In blood plasma, only 20–25% of the radioactivity was observed in the first 10 min and increased up to 40% after 90 min during the scan. In the blocking studies, the pancreatic uptake was reduced by 24% and liver uptake by 15%, after 30–60 min. In blood plasma, around 70% of the radioactivity was observed after 90 min (Figure 8).

In the non-human primate study (*n=1*), both baseline and blocking experiments were performed during the same day. In the baseline study, uptake in GK rich tissues such as pancreas and liver was higher in the monkey than in the pigs with similar bio-distribution pattern. In the blocking experiment, 0.5 mg/kg of the cold ligand (AZ12504948) was used, and the pharmacological effect of GK agonist was confirmed by a reduction in blood glucose concentration from 7.1 to 5.2 mM after 90 min. The uptake of the liver was reduced by 14% after 30–60 min post injection (p.i.), whereas no reduction was observed for pancreas after blocking (Figure 9).

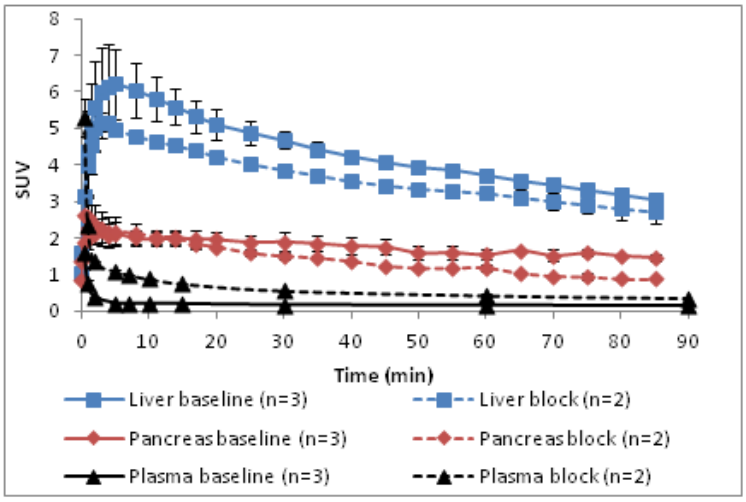

Figure 8. Tracer kinetics in liver, pancreas and blood plasma during baseline (*n=3*) and blocking scans (*n=2*) in pig. Values are expressed as SUV and given as means ± SEM.

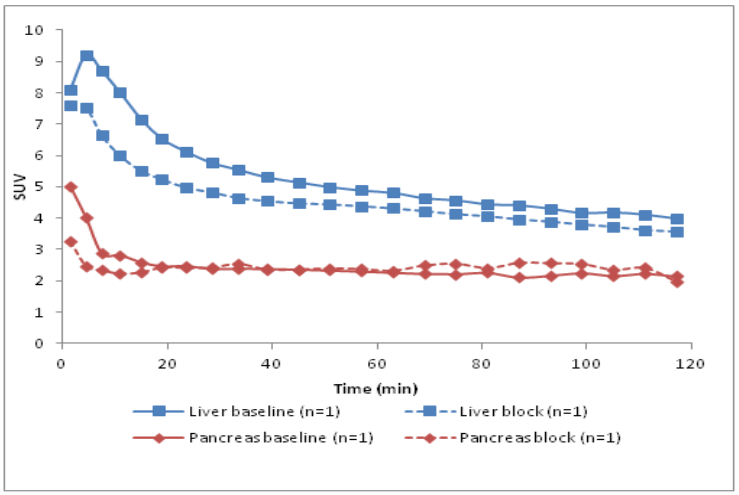

Figure 9. Tracer kinetics in liver and pancreas during baseline (*n=1*) and blocking scans (*n=1*) in non-human primate. Values are expressed as SUV.

The major route of excretion of the radioligand was through the bile system into the duodenum and large intestine, which could result in difficulty in detecting and separating the specific ligand-GK interactions in both the liver and pancreas. However, increased target specificity is required for further progress in GK imaging using PET radioligands in pancreas and liver based on this class of GK activators.

4.3 RADIOSYNTHESIS AND *IN VITRO* EVALUATION OF [^{11}C]/[^{3}H]AZ COMPOUND X IN HUMAN PANCREAS (PAPER III).

G-protein coupled receptor 44 (GPR44, also known as postaglandin D2 receptor 2) is a protein recently characterised as a highly beta cell specific surface target and absent from remaining islet cells as well as exocrine cells[209]. To generate a potential PET radioligand for visualising BCM in native pancreas, the GPR44 specific ligand, AZ Compound X, was selected and here radiolabelled with carbon-11 and tritium. The ligand was labelled using tritium, to validate and characterise the binding properties using high resolution *in vitro* ARG technique with human and rat pancreatic tissue. Similar *in vitro* binding properties were explored using the [^{11}C]AZ Compound X in post-mortem human and rat pancreatic tissue slices.

The radioligand, [^{11}C/^{3}H]AZ Compound X, was synthesised from the sodium salt of sulfinic acid precursor, in DMF using methylating agent [^{11}C/^{3}H]CH_3I in one step (Scheme 3). The radiolabelled product was formed as sulfone instead of sulfinate ester via *S*-alkylation instead of *O*-alkylation, which was in agreement with the Hard Soft Acid Base (HSAB) principle[210]. It has been shown previously that alkylation of sulfinate anion with hard alkylating agent results predominantly in ester formation, whereas soft alkylating agent such

as methyl iodide mainly results in the formation of sulfone[211], which supported our findings. In case of [^{11}C]CH_3I, methyl carbonium ion *(CH_3^+)* is attached to a soft base *Iodide (I^-)*; thus, CH_3^+ acts as a soft acid. *Co-ordination of CH_3^+* with the soft base *Sulphur (S)* is preferable compared to the harder base *Oxygen (O)* present in the precursor molecule. When more reactive methylating agent [^{11}C]CH_3OTf was used for labelling, a major radiolabelled by-product was formed. This did not co-elute with the reference standard in analytical radio-HPLC, which can be explained by formation of *O*-alkylated sulfonate ester. However, the formed radiolabelled entity was not characterised.

The conversion of [^{11}C/^{3}H]CH_3I to the product, [^{11}C/^{3}H]AZ Compound X, was almost quantitative at this condition. The total time of the radiosynthesis was 28–30 min after EOB, including online HPLC purification and formulation (PBS). The synthesis was highly reproducible; it was possible to produce up to 2500 MBq of pure product from 30 min of proton bombardment at a beam current of 35 μA. The radiochemical purity of [^{11}C]AZ Compound X was >99% up to 2 hours and >99% for [^{3}H]AZ Compound X in formulation solution, even after 1 week of EOS. The SRA of [^{11}C]AZ Compound X ranged from 900–3000 GBq/μmol and for [^{3}H]AZ Compound X was 2 GBq/μmol after EOS.

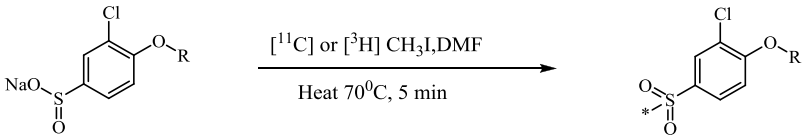

Scheme 3. Radiosynthesis of [^{11}C/^{3}H]AZ Compound X via [^{11}C/^{3}H]CH_3I.

The ARG images using [^{11}C]AZ Compound X in human pancreatic slices showed heterogeneous hotspots corresponding to islets of Langerhans in both healthy and T2DM subjects in contrast with rat pancreas, which has no GPR44 expression (used here as negative control). It was possible to almost completely block the binding to human pancreatic tissue in contrast with rat pancreatic tissue by co-incubation with 20 μM GPR44 antagonist AZ Compound Y. The enrichment in islet hotspots was >7 times higher than the exocrine background in tissues from both healthy and T2DM subjects (Figure 11). Comparable *in vitro* ARG results were found using [^{3}H]AZ Compound X (Figure 12). *In vitro* binding of [^{11}C]AZ Compound X to pancreatic tissue homogenates showed higher specificity towards islets than exocrine tissue. The specific binding was 8–20 times higher in islets of Langerhans than in exocrine preparations (Figure 13). No experiments were performed using tissue homogenates with the tritium labelled ligand. The specificity of the radioligand [^{11}C]AZ Compound X

towards islets was confirmed by insulin staining, where most of the hotspots were co-localised with insulin (Figure 14).

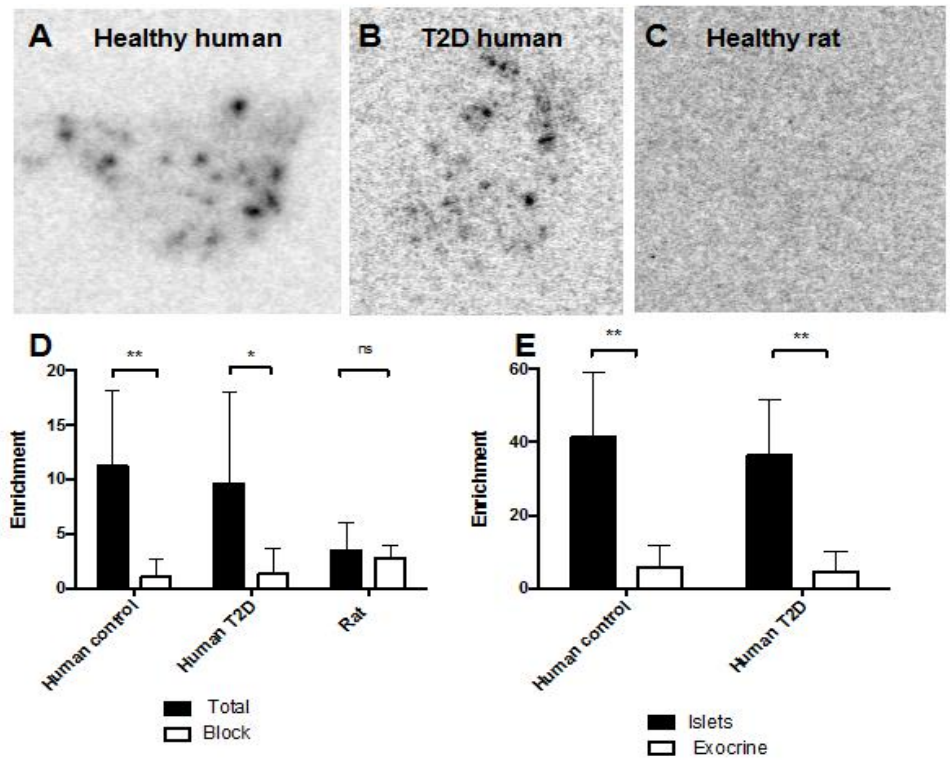

Figure 11: *In vitro* autoradiography of [^{11}C]AZ Compound X, Specific binding in pancreas from healthy human subjects (A), subjects with T2D (B) and healthy rat (C).The pancreatic binding of tracer is displaceable in human but not in rat (D), and the human pancreatic binding is concentrated to the islet of Langerhans (E).

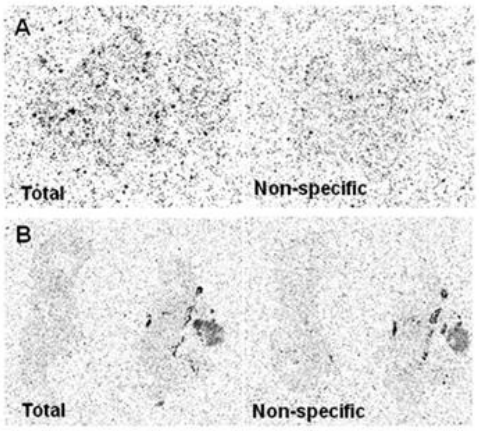

Figure *12*: *In vitro* autoradiography total binding in pancreas by 1 nM [^{3}H]AZ Compound X incubated for 3h from healthy human subjects (A) and healthy rat (B).

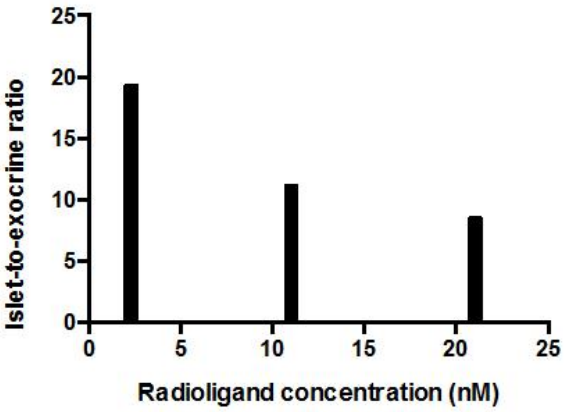

Figure 13: The islet-to-exocrine specific binding ratio was close to 20 at nanomolar concentration of radioligand [^{11}C]AZ Compound X.

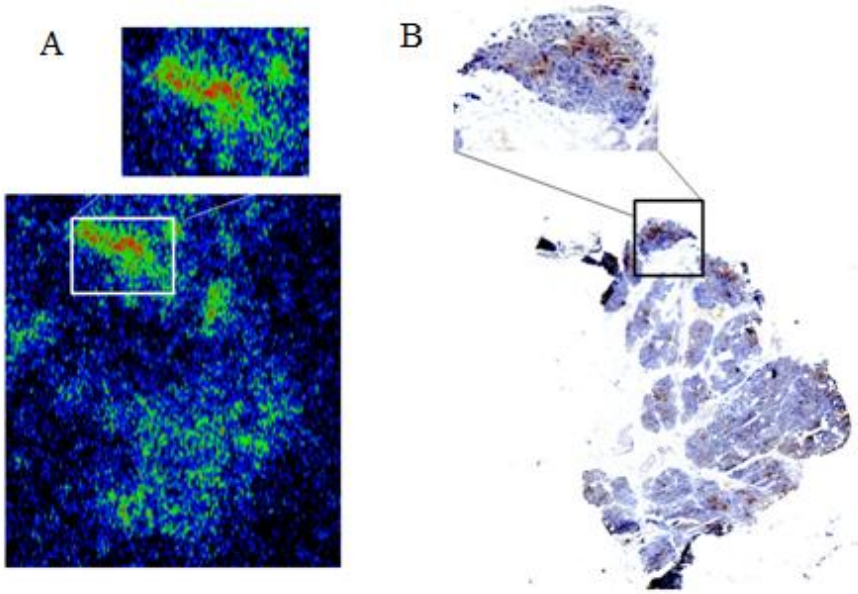

Figure 14. Autoradiogram (A) and insulin staining (B) of consecutive section of non-diabetic human pancreas show correlation of the [^{11}C]AZ Compound X tracer uptake to beta cells.

The *in vitro* binding properties of GPR44 radioligand, [^{11}C]/[^{3}H]AZ Compound X, in human pancreas and rat pancreas showed very promising results. These results motivate its further evaluation as a PET radioligand, in a preclinical setting.

4.4 FLUORINE-18 LABELLING OF THREE NOVEL D-PEPTIDES WITH [^{18}F]SFB AND EVALUATION BY WHOLE-HEMISPHERE HUMAN BRAIN SLICES AUTORADIOGRAPHY (PAPER IV)

A mirror image phase display selection approach[212] was used to find small size peptide (12-mer, a.a sequence = qshyrhispaqv, named D1) using amyloid peptide Aβ (1-42) as target. *In vitro* studies using D1-peptide labelled with fluorescence dye FITC demonstrated specific binding to Aβ plaques in brain tissue sections from former AD patients and did not bind to fibrillary deposits derived from other amyloidosis (which do not contain Aβ(1-42))[213] in contrast with Congo red, which is known to bind to any amyloid and amyloid-like fibrils, regardless of their chemical identity[213, 214]. *In vivo* studies with FITC-D1 peptide in transgenic AD model mice confirmed high specificity to dense Aβ deposits (i.e. plaques), compared to diffuse Aβ deposits[215]. Moreover, D1-peptide showed properties in reducing Aβ cell toxicity and amyloid fibril formation[216]. All data taken together demonstrates that D1-peptide or derivative of D1-peptide might be suitable for use as a molecular probe for the detection of

amyloid plaques in living humans or animals for early diagnosis of AD or to search for compounds that are suitable for AD therapy or to monitor Aβ plaque load during disease progression. In this present work, D-enantiomeric a.a was selected, since D-enantiomeric peptides are known to be less protease sensitive and more resistant to degradation in animals[217-219] than L-a.a.[220-223]. Therefore, D-peptides will be advantageous as a PET probe for visualising amyloid plaques *in vivo*. Three derivatives of D1-peptides were chosen as precursor and chemically constructed having a lysine (k) group for ^{18}F-radiolabelling by conjugation of prosthetic group [^{18}F]SFB.

Unlabelled SFB and the triflate precursor (**1**) for the radiolabelling of [^{18}F]SFB were synthesised following previously published method, with good yield[224, 225] (Scheme 4). [^{18}F]SFB was synthesised in three steps in one pot via HPLC purification before using it for the next step (^{18}F-peptide synthesis) based on the literature method, with modifications[226, 227] (Scheme 5). In our hands, purification of [^{18}F]SFB using only cartridge was not good for the ^{18}F-peptide labelling. Probably, some unidentified nonradioactive by-products, which were not removed during SPE purification of [^{18}F]SFB, affected the radiolabelling of the peptides. Dry complex of [^{18}F]F^-/K_2CO_3/$K_{2.2.2}$ was isolated in a reaction vial to which the precursor (**1**) in acetonitrile was transferred. The aromatic nucleophilic substitution reaction took place under heating and [^{18}F]**2** was formed, followed by hydrolysis using base under heating, and [^{18}F]**3** was produced. A solution of the reagent HSTU in acetonitrile was added to [^{18}F]**3,** and [^{18}F]SFB was produced under heating followed by purification on semi-preparative RP HPLC column. The fraction of [^{18}F]SFB was isolated on a SPE cartridge and eluted by acetonitrile for use in the second step. The total time of [^{18}F]SFB synthesis was 90 min from the EOB, and [^{18}F]SFB was produced in good yield (up to 3600 MBq from 15 min of irradiation, 30–35 μA). The [^{18}F]SFB was identified by analytical HPLC, comparing with the synthesised nonradioactive reference standard SFB. The radiochemical purity of [^{18}F]SFB was >98%.

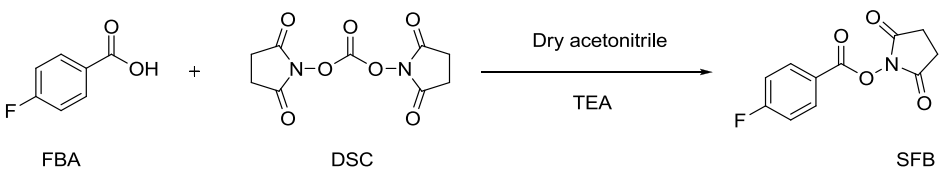

Scheme 4. Synthesis of SFB (reference of [^{18}F]SFB).

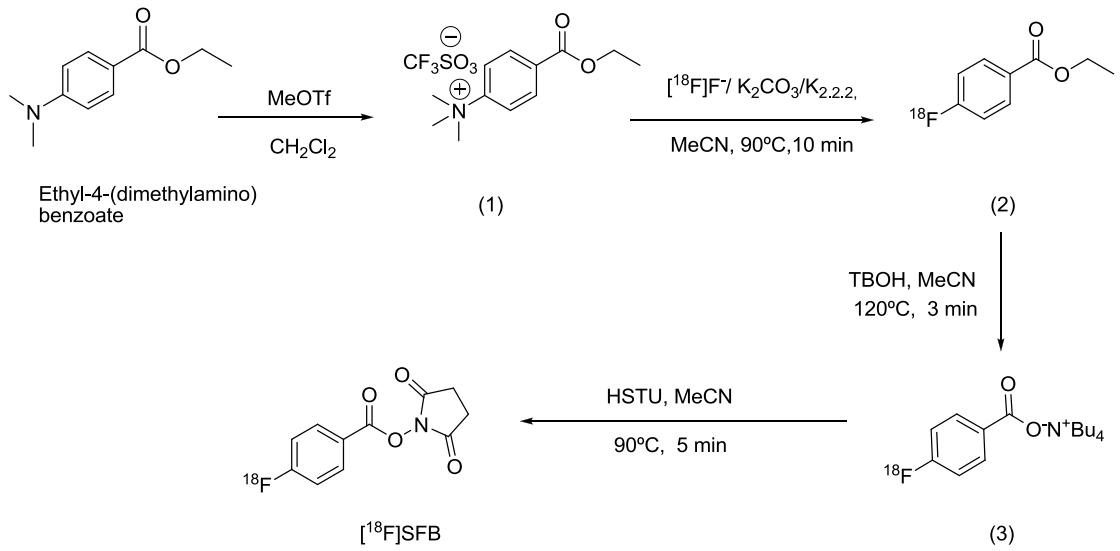

Scheme 5. Radiosynthesis of [^{18}F]SFB via^{18}F-fluoride ([^{18}F]F$^-$) by three steps in one pot.

The references, ^{19}F-peptides ([^{19}F]ACI-87-F, [^{19}F]ACI-88-F and [^{19}F]ACI-89-F), were synthesised in one step (Scheme 6) where precursor peptides were dissolved in borate buffer solution (pH~8.8) and excess amount of SFB in acetonitrile was added. The reference ^{19}F-peptides were purified by analytical HPLC system using a gradient method with acidic condition. All ^{19}F-peptides were unstable in the acidic mobile phase used during purification; therefore, purified peptide fractions were collected in a prefilled basic solution (adjusted with NaOH) in which the ^{19}F-peptides were stable. Three ^{18}F-peptides ([^{18}F]ACI-87-F or [^{18}F]ACI-88-F or [^{18}F]ACI-89-F) were radiolabelled using produced purified [^{18}F]SFB in the first step. Reaction condition for labelling was similar as the condition used for reference peptide synthesis. The incorporation yield of [^{18}F]SFB to the ^{18}F-peptides was >80% in all synthesis. Crude ^{18}F-peptides were purified by analytical HPLC system; in our hands, purification of peptides was not possible using semi-prep HPLC column. Pure fraction of ^{18}F-peptides was loaded to a SPE cartridge and eluted using EtOH and formulated in PBS solution. The formulated ^{18}F-peptides were filtered manually via a sterile filter (0.22 μm) and transferred to a sterile vial to get pyrogen free product before further use. Total time of synthesis was 40 min at the EOS of [^{18}F]SFB. The identity and radiochemical purity of ^{18}F-peptides was confirmed by analytical HPLC, comparing with the unlabelled synthesised reference peptides (^{19}F-peptides). The radiochemical purity of the formulated ^{18}F-peptides was >98% and was found to be radiochemically stable for up to 3 hours. The specific radioactivity obtained from [^{18}F]ACI-87-F was 16 GBq/μmol and 11 GBq/μmol, [^{18}F]ACI-88-F was 113 GBq/μmol and 9 GBq/μmol, [^{18}F]ACI-89-F was 86 GBq/μmol and 27 GBq/μmol.

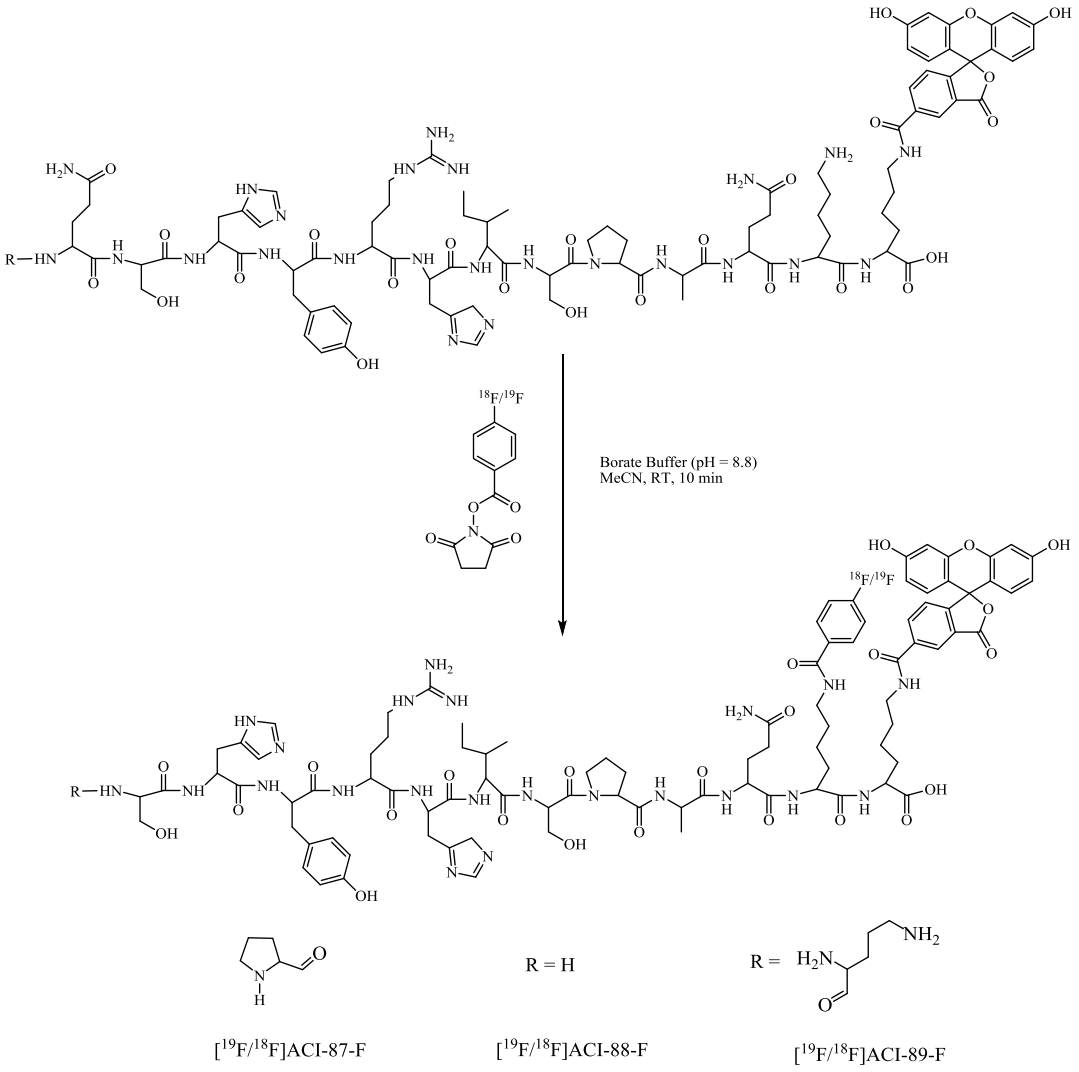

Scheme 6. Radiosynthesis of [^{18}F/^{19}F]-peptides using the prosthetic group [^{18}F/^{19}F]SFB at RT.

The *in vitro* autoradiographs of whole hemisphere human brain slices (coronal sections) of an AD patient and an age matched control (non-AD) demonstrated higher radioligand binding at the level of hippocampus. The average grey matter-white matter uptake ratios of the three D1 derivatives was also higher in AD brain than control brain slices, and [^{18}F]ACI-88-F showed the best result (Figure 15 is an example of [^{18}F]ACI-88-F). These promising *in vitro* data indicated their potential as imaging biomarkers for visualising amyloid plaques in the living brain.

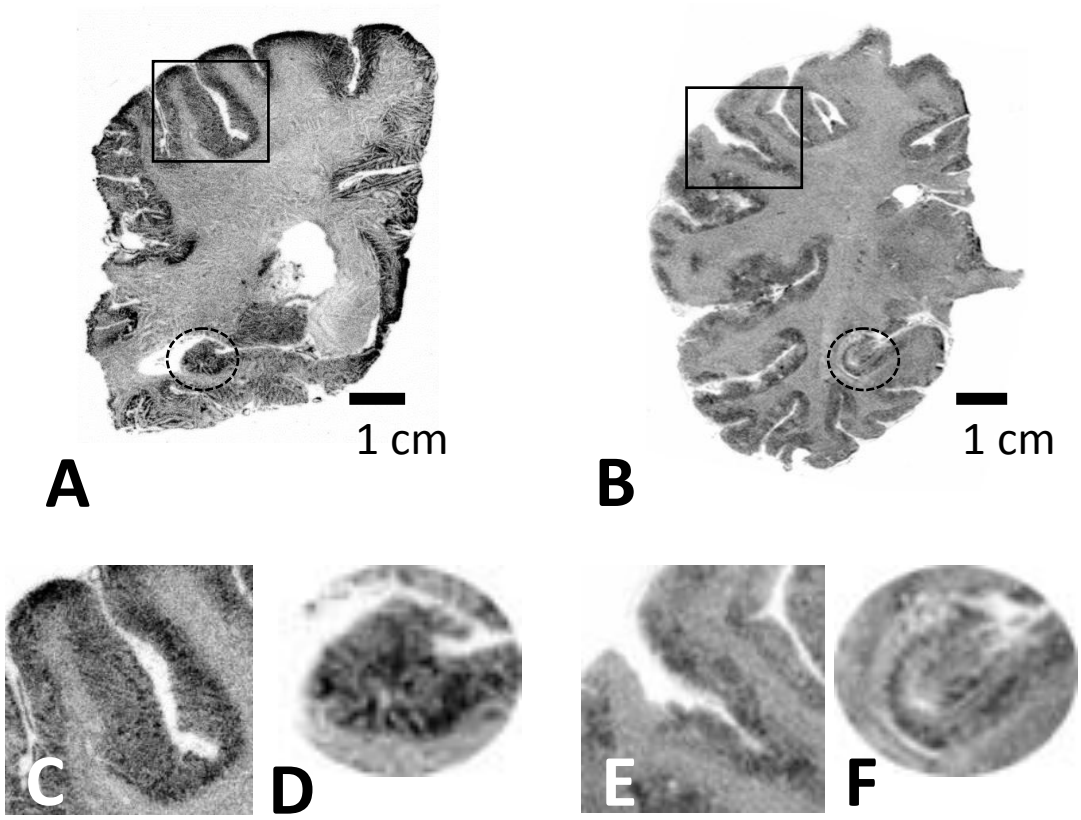

Figure 15. Whole hemisphere coronal autoradiographs, using [^{18}F]ACI-88-F as radioligand, brain of a 50-year-old female with AD (A) and a 54-year-old male control (B). Higher binding in the grey matter and in the hippocampus was observed in AD slice compared to the control (darker colour indicates higher radioligand uptake). Panels (C) and (E) represent the enlargements, indicated by the rectangular image boxes in panels (A) and (B).

5 SUMMARY OF FINDINGS

The present thesis focused on development of small molecule PET probes for BCM imaging and development of peptide molecule (12-amino acid), PET probes, for Aβ plaque imaging in the brain.

Firstly, a fluorinated analogue of the VMAT2 radioligand DTBZ was developed. In order to reduce the rate of *in vivo* defluorination of previously published radioligand, [^{18}F]FE-DTBZ, isotopic substitution of the four hydrogen atoms on the ^{18}F-ethyl group with deuterium was performed and tested, both *in vitro* and *in vivo* by PET. [^{18}F]FE-DTBZ-d4, was radiolabelled in two steps from optically resolved 9-*O*-desmethyl-*(+)*-DTBZ precursor using the prosthetic group, deuterated [^{18}F]fluoroethylbromide [^{18}F]FEtBr-d_4, at *O*-position by nucleophilic alkylation reaction. The *in vivo* stability of the novel radioligand [^{18}F]FE-DTBZ-d4 has improved notably through the deuterium isotopic effect, since cleavage of C-D bond via enzymatic attack is more difficult to break than C-H bond. However, our findings suggest that [^{18}F]FE-DTBZ-d4 is not a suitable PET radioligand for endogenous BCM imaging in pancreas due to high nonspecific interactions *in vivo* obscuring the islet signals.

Secondly, carbon-11 labelled small molecule glucokinase activator, [^{11}C]AZ12504948, was synthesised from its aliphatic desmethyl precursor using [^{11}C]methyl iodide, [^{11}C]CH_3I. Alkylation of the *O*-position via nucleophilic substitution reaction was successful without masking the amide group present in the precursor molecule. Radioligand [^{11}C]AZ12504948 was evaluated both *in vitro* and *in vivo* by autoradiography (ARG) and PET, respectively, to visualise intracellular target enzyme glucokinase in the liver and pancreas. These studies confirmed the specificity of the radioligand was too low to provide clear signal to noise ratio.

Thirdly, a small molecule GPR44 specific ligand, AZ compound X, was radiolabelled using both carbon-11 and tritium radionuclides, from the sodium sulfinic acid salt precursor, using [^{11}C/^{3}H]CH_3I for visualising BCM in pancreas. The *in vitro* binding studies using ARG technique demonstrated binding with high specificity to human islets of pancreatic tissues, which seems promising for further evaluation *in vivo*. The presence of islets was confirmed by insulin staining, using sequential human pancreatic slices used for ARG.

Finally, three different fluorine-18 labelled D-peptides were developed and radiolabelled using prosthetic group [^{18}F]SFB, for visualising amyloid plaques in the human brain by PET. *In vitro* ARG studies demonstrated higher accumulation of the ^{18}F-peptides in Alzheimer's disease (AD) brain tissue slices compared to that of age-matched control non-AD individual, and one of these three ^{18}F-peptides was proven to be the best candidate for further evaluation *in vivo*.

6 FUTURE PERSPECTIVE AND CHALLENGES

To find an ideal radioligand for beta cell mass (BCM), imaging has already been proven to be a difficult task compared to other research areas. The main challenge in beta cell imaging (BCI) is the small volume (1–2%) of endocrine tissue and heterogeneity of islets throughout the exocrine pancreas[228], in contrast with tumour imaging where the target of interest is over expressed. The second challenge is the location of the pancreas, which is surrounded by the liver and gastrointestinal system; thereby, excretion route is considered to be an obstacle. The hepatobilary excretion of radioligand or radiometabolites results in enhanced non-target radioactivity concentrations in the intestinal tract, which makes delineation of the pancreatic uptake difficult. The sensitivity of PET imaging is dependent on the endogenous expression level of the target protein and the specificity, as well as binding affinity of the radioligand with high specific radioactivity. Thus, it is critical to develop radionuclide probes with high contrast and beta cell specificity with favourable pharmacokinetics. A recent theoretical quantitative analysis of non-invasive BCM imaging was published[166], where they estimated that the specificity of the radioligand towards β-cells should be 100-fold to 1000-fold more than exocrine cells (volume fraction of β-cells and exocrine cells; 1:100). With the progression of the disease i.e. decrease of BCM, the specificity of the radioligand for β-cells increases exponentially. This is an achievement difficult for any radioligand. In any case, in spite of severe methodological challenges, progress has been documented for BCM imaging using PET technique. None of the methods available so far has proven to predict BCM with a comparable accuracy as the functional PET method applied herein[162, 165-167]. It is important to emphasise that significant efforts have recently been underway to identify β-cell specific targets and to design as highly specific radioligands to these targets as possible. In the present work, three novel PET radioligands were developed for three different molecular targets and explored for BCM imaging in order to contribute to the development of so called “ideal” radioligand to gain knowledge about diabetes and to assist patients with personalised medical care as well as to advance drug discovery, which is finally *the ultimate goal*.

Vesicular monoamine transporter type 2 (VMAT2) is a target for imaging BCM, and radioligand dihydrotetrabenazine (DTBZ) binds specifically to target VMAT2. Hepatic islet transplantation is suffering from poor long-term outcome and graft failure due to inadequate graft revascularisation. DTBZ-based radioligands are out of reach to follow hepatic islet transplantation, since the liver is responsible for many metabolic pathways i.e. high non-target signals. Currently, new transplanted sites have been evaluated for increased graft

survival, and outcome tissues are bone marrow and brachioradialis (forearm muscle). Our developed novel radioligand, [^{18}F]FE-DTBZ-d4, has the characteristics considering the study to VMAT2 dense tissue in proximity to cortical bone structure such as intramuscular islet transplantation in clinical and preclinical settings.

The GPR44 receptor, which is highly expressed on the surface of the β-cells in pancreas seems a very attractive target for BCI. Based on our experiments, the developed GPR44 specific radioligand (AZ compound X) demonstrated high specificity towards the islets of human pancreas *in vitro*. The *in vivo* PET studies in preclinical settings are highly desirable to validate this radioligand, in non-diabetic large animals for visualisation and quantification of BCM in pancreas. To confirm the specificity of the radioligand, pretreatment or displacement studies with cold ligand is required. In order to be able to follow the small difference of radioligand uptake in the pancreas of non-diabetic and diabetic subjects i.e. BCM, type 1 diabetic model of animal is essential. Unfortunately, GPR44 is not expressed in rat pancreas, as several rodent diabetes models are available. Therefore, pig models of T1DM or T2DM could be utilised for *in vivo* evaluation of [^{11}C]AZ Compound X similarly by following previously evaluated method[229]. Radiometabolite analysis of [^{11}C]AZ Compound X needs to be performed to follow the stability of the parent radioligand throughout the PET scan, especially for the kinetic modelling quantification.

The main challenge in case of labelled peptide for brain PET imaging is the blood-brain-barrier (BBB) penetration compared to small molecules. Poor distribution to the brain and high nonspecific binding is the main reason for failure of useful CNS radioligands. Substances that are able to inhibit Aβ aggregation and reduce its toxic effects are still highly desirable for diagnosis and potential therapy. *In vitro* studies of three ^{18}F-D-peptides using ARG technique demonstrated high specificity towards Aβ plaques of AD patient's brain slices compared to non-AD subject, which makes them have a potential for further evaluation *in vivo* by highly sensitive PET imaging techniques. Our preliminary results of dynamic PET (*in vivo*) studies in cynomolgus monkey brain, using these three ^{18}F-D-peptides, demonstrated low brain penetration (in the range of 0.1 % of the injected dose corrected for blood volume and arterial blood concentration), which makes these ^{18}F-peptides unsuitable as PET probe in its current form. The study of metabolism of three ^{18}F-D-peptides during the PET experiments showed very high stability and metabolic resistance. In conclusion, desired modification of D-enantiomeric peptide (which is fully synthetic) is necessary to improve the properties to cross the BBB for future PET studies in order to visualise amyloid plaques in AD brain.

7 ACKNOWLEDGEMENTS

This thesis was made possible by the direct or indirect help and support from numerous people. I would specially like to thank:

First of all, I would like to express my sincere gratitude to my world-renowned supervisor Prof. Christer Halldin for accepting me as a PhD student in your group. I feel so proud to be a part of your famousness. Everybody knows about you in the radiochemistry field and I will always carry a piece of your fame wherever I go, after getting the PhD degree under your supervision. Thanks for being there, supporting me and encouraging me when I needed it the most, and for being so enthusiastic about my work, no matter where you were in the world! Your positive way of looking at life and work, your openness to accept my opinion with great consideration, your belief on my "research, productions and writings" gave me so much strength to solve many challenges I faced during my working life at KI. Thank you! "You do really care about your PhD student's wellbeing".

Thanks to my co-supervisor, Dr. Peter Johnström for your constructive criticism, reviewing my thesis with special care and to share knowledge about radiochemistry and drug development whenever you had time. My co-supervisor Dr. Olof Eriksson; you are the rising star of BCM imaging; you will reach the top. Your guidance and helpfulness regarding our radioligands application taught me enough about diabetes and the pancreas and gave me the confidence to face my defense discussion about PET imaging. Dr. Lars Johansson, for your avid involvement in BCM project from 2008-2014.

My expert co-workers at Karolinska PET group from whom I have learned so much; Dr. Kenneth Dahl; for your technical assistance, helpful approach to coach new equipments with patience and for creating a nice working and friendly environment. Dr. Sangram Nag; your knowledge about chemistry and your optimistic and cooperative nature constantly amaze me. You always have answers to all of my questions and come up with solutions for anything from radiochemistry to technical matters. Dr. Magnus Schou; for your politeness, discussions about radiochemistry and your jokes which gave some brightness at regular and late evening working hours. Dr. Zhisheng Jia; your helpfulness and effectiveness during productions as well as research are always enjoyable; it has been a pleasure to work with you. Dr. Raisa Krasikova; for your valuable scientific discussions and willingness to share your knowledge about radiochemistry. Arsalan Amir; for your technical assistance with QC and productive suggestions on improving quality of life and work, Guennadi Jogolev; for your technical assistance with QC and co-operation in the lab. Past and present members of KI PET group: Dr. Jan Andersson; for being such a nice and kind colleague and for also being a great listener, Dr. Sjoerd J. Finnema; for your valuable conversation about science and life, Carsten Steiger; for being a great office-mate and sharing your knowledge from radiochemistry to quality control. Dr. Arindam Das, Johan Ullin, Anton Lindberg, Petra Agirman, Youssef EL Khoury, Dr. Vladimir Stepanov, Maria Yakovleva, Hanna I. Jacobsson, Andreas Westermark, Nandoor Kapósy, Henrik Alfredéen, Dr. Pavitra Kannan, Steffan Martinsson, Ana Maria, Mahdi Moein and Antonio Bermejo for keeping up a pleasant atmosphere in the office corridor.

Dr. Balazs Gulyás, Dr. Marie Svedberg, Åsa Södergren and Siv Eriksson; for sharing your expertise and assistance with autoradiography experiments and data analysis. Dr. Akihiro Takano for sharing your expertise in NHP experiments and data analysis. Dr. Nahid Amini and Dr. Ryuji Nakao for assistance with radiometabolite and LC-MS analysis. Madjid Ebrahimi-Mehrabani and Phong Truong for your friendship and constant support with the cyclotron. Dr. Ram Kumar Selvaraju for your assistance with the in vitro experiments and data analysis, for your friendship and valuable comments about my thesis. Karin Zahir, for your administrative assistance concerning both personal and work-related issues, and for your loving care. Urban Hansson, for all the IT support and positive energy.

Dr. Martin Schain, Dr. Anton Forsberg, Dr. Magdalena Nord, Granville Matheson, Pontus P. Sigray, Dr. Miklós Tóth, Dr. Jenny Häggkvist, Lenke Tari, Pauliina Ikonen, Karin Collste, Dr. Mikael Tiger, Dr. Simon Cervenka, Dr. Jacqueline Borg, Dr. Johan Lundberg, Patrik Fazio, Emma Veldman, Max Andersson; for providing such a friendly and welcoming atmosphere at lunch. No matter if you were in the middle of a conversation, whether you were talking about science or movies or sports, you always had time to welcome any newcomer into the discussion or make space at a crowded table. You could be a role model for any group, when it comes to integrating many people who come from different parts of the world! Being away from home many years, missing all my friends and lunchtime discussions, you gave me that taste of home!

Dr. Lars Farde, Dr. Andrea Varrone, Dr. Per Stenkrona, Dr. Katarina Varnäs, Göran Rosenqvist, Dr. Rafael Maior, Nina Knave, Jonas Ahlgren, Gudran Nylen, Ryosuke Arakawa, Kai-Chun Yang, Anne Bystrom, Emma Meyer, Hanna Elgstrand for your support and comforting atmosphere. Kia Hultberg-Lundberg; for all your support when my mom was visiting, Opokua Britton; for nail art talk, Karin Olsson; for your love and being Leeba's extra Grandma, Sara Lundqvist and Zsolt Sarnyai for your friendly activities.

Members of the PET Neuroradiology group, Prof. Sharon Stone-Elander, Dr. Jan-Olov Thorell, Dr. Erik Samén, Dr. Obaidur Rahman, Emma Jussing, Johanna Backström, Rebecka Dahlfors, Marléne Dilenstam, Seth Björk for keeping smooth co-operation in the radiochemistry labs.

Thanks to Prof. Bengt Långström for introducing me with this fascinating radiochemistry world; for providing outstanding working facilities and made me feel very welcome in your group during my M.Sc. thesis work at Uppsala University. Thanks to Prof. Ian Nicholls and Assoc. Prof. Susanne Wikman; for your warm welcome and generosity during my short-stay at Kalmar University. Prof. Jean DaSilva for your supervision and hospitality all through my work at the University of Ottawa Heart Institute and to Dr. Tayebeh Hadizad; for your support at UOHI lab and friendship.

My friends from Sweden: Magdalena for being so true friend and always being there for me whenever I needed, both for laughter and sorrow. Marie, for sharing your wisdom and exclusive books from your rich library. I have learned many things from you and constantly learning. I am so blessed to have friends like you around me here in Sweden where I can go whenever I feel down. Kristofer, Bernt, Pamela, Emo, Kazi and Ratan vai for being around.

My friends of Chemistry Department and Science faculty of Dhaka University; I miss you intensely, all the chit-chat around Carzon hall, the tea breaks, lunch breaks, new year's celebration, book fair, study tour, watching cricket, all the fun we had together. Those long hours in the library studying for our exams, making notes, long intensive theory and practical classes from 8-17 everyday, I wouldn't have survived without you guys through those long years. Special thanks to Mahbub, I would have dropped out from studying Chemistry in the 1st year, if you had not been there! Ehsan for your great help and support for taking care of my family in Dhaka when I wasn't around, it means a lot to me. Nipa, Nila, Monzur for keeping your friendship. Thanks to Ma, Bapi, Dada, Shiuly di, Biku, Popy for giving me a new family.

Thanks to all my excellent scholar cousins and family members who always inspired me to be one of them! I am lucky to have such a family who were giving me fuel all the time, special thanks to my uncle Fazlul Hoque and aunt Taslimah, Swapan, Shaku, Himu, Tanvir and Shahin dada, Liton vai, Lopa, Tania, Miki, Jerin and Shamu apu, Juthy, Anik, Shoumik, Shoily, Shoha, Tisha, Arham, Reem, Mahadia and all of you that I didn't mention herein.

My parents and family; My father, who is not here anymore to share my achievement, would be so proud of me today; thanks to him and my mother for your enormous support, inspiration and forgiveness. I know I wasn't always easy to handle, my stubbornness and independent way of thinking upset you at times, but in the end you have proven that "love and affection" is stronger than anything else! To my only sister Poly for your encouragement and strong influence all through my life, to my elder brother Murad for your kindness and love, My younger brothers Babu and Sharnav; for your undying support throughout the years, your patience and taking so great care of our parents in our absence; it is not so easy to live far from home and not to be able to contribute when you need the most. I love you all with my heart.

My dear husband Sangram, I don't know where to start and where to end; you are the rock upon which I stand! Without your love, your endless patience and support, it would not be possible to accomplish this thesis. You have taken such great care of me and Leeba. From the time you and Leeba came into my life, I feel complete and now with this PhD, I feel satisfied. I am sure after these all painful months, you have learned what Islets of Langerhans is and Leeba has learned to say "Mummy, I have a small Pancreas".

My sweet daughter Leeba: you are my sunshine; you are the best thing that has ever happened to me ☺.

Mahabuba (Jolly)

Stockholm, August 2016

8 REFERENCES

1. Hevesy GV, Paneth F. The solubility of lead sulfide and lead chromate. *Zeitschrift für anorganische Chemie*. 1913;82(1):323-328.

2. Hevesy G. The Absorption and Translocation of Lead by Plants: A Contribution to the Application of the Method of Radioactive Indicators in the Investigation of the Change of Substance in Plants. *Biochem J*. 1923;17(4-5):439-445.

3. Hevesy GC, Smedley-Maclean I. The synthesis of phospholipin in rats fed on the fat-deficient diet. *Biochem J*. Jun 1940;34(6):903-905.

4. Joliot F, Curie I. Artificial Production of a New Kind of Radio-Element. *Nature*. Mar 1934;133(3354):201.

5. Lawrence EO, Sloan DH. The Production of High Speed Canal Rays without the Use of High Voltages. *Proc Natl Acad Sci U S A*. Jan 1931;17(1):64-70.

6. Livingston MS, Henderson MC, Lawrence EO. Radioactivity Artificially Induced by Neutron Bombardment. *Proc Natl Acad Sci U S A*. Aug 1934;20(8):470-475.

7. Ametamey SM, Honer M, Schubiger PA. Molecular imaging with PET. *Chem Rev*. May 2008;108(5):1501-1516.

8. Weissleder R, Mahmood U. Molecular imaging. *Radiology*. May 2001;219(2):316-333.

9. Wagner HN, Szabo Z. *Principles* of *Nuclear Medicine*. *Philadelphia: W.B.Saunders Company*. Jul 2008;2nd:178-194.

10. Cherry SR, Gambhir SS. Use of positron emission tomography in animal research. *ILAR J*. 2001;42(3):219-232.

11. Eriksson L, Dahlbom M, Widen L. Positron emission tomography-a new technique for studies of the central nervous system. *J Microsc*. Mar 1990;157(Pt 3):305-333.

12. Ter-Pogossian MM, Phelps ME, Hoffman EJ, Mullani NA. A positron-emission transaxial tomograph for nuclear imaging (PETT). *Radiology*. Jan 1975;114(1):89-98.

13. Phelps ME, Hoffman EJ, Huang SC, Ter-Pogossian MM. Effect of positron range on spatial resolution. *J Nucl Med*. Jul 1975;16(7):649-652.

14. Phelps ME, Hoffman EJ, Mullani NA, Ter-Pogossian MM. Application of annihilation coincidence detection to transaxial reconstruction tomography. *J Nucl Med*. Mar 1975;16(3):210-224.

15. Wagner HN, Jr. Clinical PET: its time has come. *J Nucl Med*. Apr 1991;32(4):561-564.

16. Ido T, Wan CN, Casella V, Fowler JS, Wolf AP, Reivich M, Kuhl DE. Labeled 2-deoxy-D-glucose analogs. ^{18}F-labeled 2-deoxy-2-fluoro-D-glucose, 2-deoxy-2-fluoro-D-mannose and ^{14}C-2-deoxy-2-fluoro-D-glucose. *Journal of Labelled Compounds and Radiopharmaceuticals*. 1978;14(2):175-183.

17. Di Chiro G. Positron emission tomography using [^{18}F]fluorodeoxyglucose in brain tumors. A powerful diagnostic and prognostic tool. *Invest Radiol*. May 1987;22(5):360-371.

18. Wagner HN, Jr., Conti PS. Advances in medical imaging for cancer diagnosis and treatment. *Cancer*. Feb 15 1991;67(4 Suppl):1121-1128.

19. Nieweg OE, Kim EE, Wong WH, Broussard WF, Singletary SE, Hortobagyi GN, Tilbury RS. Positron emission tomography with fluorine-18-deoxyglucose in the detection and staging of breast cancer. *Cancer*. Jun 15 1993;71(12):3920-3925.

20. Duhaylongsod FG, Lowe VJ, Patz EF, Jr., Vaughn AL, Coleman RE, Wolfe WG. Detection of primary and recurrent lung cancer by means of F-18 fluorodeoxyglucose positron emission tomography (FDG PET). *J Thorac Cardiovasc Surg*. Jul 1995;110(1):130-139; discussion 139-140.

21. Basu S, Alavi A. Unparalleled contribution of ^{18}F-FDG PET to medicine over 3 decades. *J Nucl Med*. Oct 2008;49(10):17N-21N, 37N.

22. Morrish PK, Rakshi JS, Bailey DL, Sawle GV, Brooks DJ. Measuring the rate of progression and estimating the preclinical period of Parkinson's disease with [^{18}F]dopa PET. *J Neurol Neurosurg Psychiatry*. Mar 1998;64(3):314-319.

23. Tolboom N, Yaqub M, van der Flier WM, Boellaard R, Luurtsema G, Windhorst AD, Barkhof F, Scheltens P, Lammertsma AA, van Berckel BN. Detection of Alzheimer pathology in vivo using both [^{11}C]PIB and [^{18}F]FDDNP PET. *J Nucl Med*. Feb 2009;50(2):191-197.

24. Cherry SR. Fundamentals of positron emission tomography and applications in preclinical drug development. *J Clin Pharmacol*. May 2001;41(5):482-491.

25. Knaapen P, de Haan S, Hoekstra OS, Halbmeijer R, Appelman YE, Groothuis JG, Comans EF, Meijerink MR, Lammertsma AA, Lubberink M, Gotte MJ, van Rossum AC. Cardiac PET-CT: advanced hybrid imaging for the detection of coronary artery disease. *Neth Heart J*. Feb 2010;18(2):90-98.

26. Farde L, Hall H. Positron emission tomography--examination of chemical transmission in the living human brain. Development of radioligands. *Arzneimittelforschung*. Feb 1992;42(2A):260-264.

27. Halldin C, Gulyas B, Farde L. PET studies with carbon-11 radioligands in neuropsychopharmacological drug development. *Curr Pharm Des*. Dec 2001;7(18):1907-1929.

28. Lee CM, Farde L. Using positron emission tomography to facilitate CNS drug development. *Trends Pharmacol Sci*. Jun 2006;27(6):310-316.

29. Bauer M, Wagner CC, Langer O. Microdosing studies in humans: the role of positron emission tomography. *Drugs R D*. 2008;9(2):73-81.

30. Wagner CC, Langer O. Approaches using molecular imaging technology -- use of PET in clinical microdose studies. *Adv Drug Deliv Rev*. Jun 19 2011;63(7):539-546.

31. Bergström M, Grahnen A, Långström B. Positron emission tomography microdosing: a new concept with application in tracer and early clinical drug development. *Eur J Clin Pharmacol*. Sep 2003;59(5-6):357-366.

32. Dimasi JA. Risks in new drug development: approval success rates for investigational drugs. *Clin Pharmacol Ther*. May 2001;69(5):297-307.

33. Matthews PM, Rabiner EA, Passchier J, Gunn RN. Positron emission tomography molecular imaging for drug development. *Br J Clin Pharmacol*. Feb 2012;73(2):175-186.

34. Smith DF, Stork BS, Wegener G, Jakobsen S, Bender D, Audrain H, Jensen SB, Hansen SB, Rodell A, Rosenberg R. Receptor occupancy of mirtazapine determined by PET in healthy volunteers. *Psychopharmacology (Berl)*. Nov 2007;195(1):131-138.

35. Farde L, Hall H, Ehrin E, Sedvall G. Quantitative analysis of D2 dopamine receptor binding in the living human brain by PET. *Science*. Jan 17 1986;231(4735):258-261.

36. Halldin C, Farde L, Hogberg T, Mohell N, Hall H, Suhara T, Karlsson P, Nakashima Y, Swahn CG. Carbon-11-FLB 457: a radioligand for extrastriatal D2 dopamine receptors. *J Nucl Med*. Jul 1995;36(7):1275-1281.

37. Halldin C, Stone-Elander S, Farde L, Ehrin E, Fasth KJ, Langstrom B, Sedvall G. Preparation of ^{11}C-labelled SCH 23390 for the in vivo study of dopamine D-1 receptors using positron emission tomography. *Int J Rad Appl Instrum A*. 1986;37(10):1039-1043.

38. Farde L, Nordstrom AL, Wiesel FA, Pauli S, Halldin C, Sedvall G. Positron emission tomographic analysis of central D1 and D2 dopamine receptor occupancy in patients treated with classical neuroleptics and clozapine. Relation to extrapyramidal side effects. *Arch Gen Psychiatry*. Jul 1992;49(7):538-544.

39. Farde L, Nordstrom AL. PET examination of central D2 dopamine receptor occupancy in relation to extrapyramidal syndromes in patients being treated with neuroleptic drugs. *Psychopharmacol Ser*. 1993;10:94-100.

40. Kapur S, Zipursky R, Jones C, Remington G, Houle S. Relationship between dopamine D(2) occupancy, clinical response, and side effects: a double-blind PET study of first-episode schizophrenia. *Am J Psychiatry*. Apr 2000;157(4):514-520.

41. Levin CS. Primer on molecular imaging technology. *Eur J Nucl Med Mol Imaging*. Dec 2005;32 Suppl 2:S325-345.

42. Ollinger JM. Estimation algorithms for dynamic tracer studies using positron-emission tomography. *IEEE Trans Med Imaging*. 1987;6(2):115-125.

43. https://en.wikipedia.org/wiki/Positron_emission_tomography.

44. Halldin C, Gulyas B, Langer O, Farde L. Brain radioligands--state of the art and new trends. *Q J Nucl Med*. Jun 2001;45(2):139-152.

45. Långström B, Bergson G. The determination of optimal yields and reaction-times in synthesis with short-lived radionuclides of high specific activity. *Radiochemical and Radioanalytical Letters*. 1980;43(1):47-54.

46. Långström B, Obenius U, Sjöberg S, Bergson G. Kinetic aspects of the synthesis using short-lived radionuclides. *Journal of Radioanalytical Chemistry*. 1981;64(1-2):273-280.

47. Långström B, Kihlberg T, Bergström M, Antoni G, Bjorkman M, Forngren BH, Forngren T, Hartvig P, Markides K, Yngve U, Ogren M. Compounds labelled with short-lived beta(+)-emitting radionuclides and some applications in life sciences. The importance of time as a parameter. *Acta Chem Scand*. Sep 1999;53(9):651-669.

48. Thorell J-O, Stone-Elander S, Elander N. Use of a microwave cavity to reduce reaction times in radiolabelling with [^{11}C]cyanide. *Journal of Labelled Compounds and Radiopharmaceuticals*. 1992;31(3):207-217.

49. Pike VW. Positron-emitting radioligands for studies in vivo-probes for human psychopharmacology. *J Psychopharmacol*. Jan 1993;7(2):139-158.

50. Mintun MA, Raichle ME, Kilbourn MR, Wooten GF, Welch MJ. A quantitative model for the in vivo assessment of drug binding sites with positron emission tomography. *Ann Neurol*. Mar 1984;15(3):217-227.

51. Dickson CJ, Gee AD, Bennacef I, Gould IR, Rosso L. Further evaluation of quantum chemical methods for the prediction of non-specific binding of positron emission tomography tracers. *Phys Chem Chem Phys*. Dec 28 2011;13(48):21552-21557.

52. Patel S, Gibson R. In vivo site-directed radiotracers: a mini-review. *Nucl Med Biol*. Nov 2008;35(8):805-815.

53. Waterhouse RN. Determination of lipophilicity and its use as a predictor of blood-brain barrier penetration of molecular imaging agents. *Mol Imaging Biol*. Nov-Dec 2003;5(6):376-389.

54. Li Z, Wang X, Xu X, Yang J, Qiu Q, Qiang H, Huang W, Qian H. Design, synthesis and structure-activity relationship studies of novel phenoxyacetamide-based free fatty acid receptor 1 agonists for the treatment of type 2 diabetes. *Bioorg Med Chem*. Oct 15 2015;23(20):6666-6672.

55. Leo A, Hansch C, Elkins D. Partition coefficients and their uses. *Chemical Reviews*. 1971;71(6):525-616.

56. http://www.acdlabs.com.

57. Osman S, Lundkvist C, Pike VW, Halldin C, McCarron JA, Swahn CG, Farde L, Ginovart N, Luthra SK, Gunn RN, Bench CJ, Sargent PA, Grasby PM. Characterisation of the appearance of radioactive metabolites in monkey and human plasma from the 5-HT1A receptor radioligand, [^{11}C]WAY-100635--explanation of high signal contrast in PET and an aid to biomathematical modelling. *Nucl Med Biol*. Apr 1998;25(3):215-223.

58. Schou M, Halldin C, Pike VW, Mozley PD, Dobson D, Innis RB, Farde L, Hall H. Post-mortem human brain autoradiography of the norepinephrine transporter using (S,S)-[^{18}F]FMeNER-D2. *Eur Neuropsychopharmacol*. Oct 2005;15(5):517-520.

59. Fowler JS, Wolf AP, MacGregor RR, Dewey SL, Logan J, Schlyer DJ, Långström B. Mechanistic positron emission tomography studies: demonstration of a deuterium isotope effect in the monoamine oxidase-catalyzed binding of [^{11}C]L-deprenyl in living baboon brain. *J Neurochem*. Nov 1988;51(5):1524-1534.

60. Halldin C, Swahn CG, Farde L, Sedvall G. Radioligand disposition and metabolism. *Kluwer Academic Publishers*. Dec 1995:55.

61. Zoghbi SS, Shetty HU, Ichise M, Fujita M, Imaizumi M, Liow JS, Shah J, Musachio JL, Pike VW, Innis RB. PET imaging of the dopamine transporter with [^{18}F]FECNT: a polar radiometabolite confounds brain radioligand measurements. *J Nucl Med*. Mar 2006;47(3):520-527.

62. Gourand F, Amini N, Jia Z, Stone-Elander S, Guilloteau D, Barre L, Halldin C. [^{11}C]MADAM Used as a Model for Understanding the Radiometabolism of Diphenyl Sulfide Radioligands for Positron Emission Tomography (PET). *PLoS One*. 2015;10(9):e0137160.

63. Andersson JD, Seneca N, Truong P, Wensbo D, Raboisson P, Farde L, Halldin C. Palladium mediated [^{11}C]cyanation and characterization in the non-human primate brain of the novel mGluR5 radioligand [^{11}C]AZD9272. *Nucl Med Biol*. May 2013;40(4):547-553.

64. Kihlberg T, Karimi F, Långström B. [^{11}C]Carbon monoxide in selenium-mediated synthesis of [^{11}C]carbamoyl compounds. *J Org Chem*. May 31 2002;67(11):3687-3692.

65. Nordeman P, Estrada S, Odell LR, Larhed M, Antoni G. [^{11}C]-Labeling of a potent hydroxyethylamine BACE-1 inhibitor and evaluation in vitro and in vivo. *Nucl Med Biol*. Jul 2014;41(6):536-543.

66. Larsen P, Ulin J, Dahlström K, Jensen M. Synthesis of [^{11}C]iodomethane by iodination of [11C]methane. *Applied Radiation and Isotopes*. 1997;48(2):153-157.

67. Andersson J, Truong P, Halldin C. In-target produced [^{11}C]methane: Increased specific radioactivity. *Appl Radiat Isot*. Jan 2009;67(1):106-110.

68. Långström B, Lundqvist H. The preparation of ^{11}C-methyl iodide and its use in the synthesis of [^{11}C]-methyl-L-methionine. *Int J Appl Radiat Isot*. Jul 1976;27(7):357-363.

69. Comar D, Cartron J, Maziere M, Marazano C. Labelling and metabolism of methionine-methyl-^{11}C. *Eur J Nucl Med*. 1976;1(1):11-14.

70. Link JM, Krohn KA, Clark JC. Production of [^{11}C]CH_3I by single pass reaction of [^{11}C]CH_4 with I_2. *Nucl Med Biol*. Jan 1997;24(1):93-97.

71. Miller PW, Bender D. [^{11}C]carbon disulfide: a versatile reagent for PET radiolabelling. *Chemistry*. Jan 9 2012;18(2):433-436.

72. Någren K, Halldin C. Methylation of amide and thiol functions with [^{11}C]methyl triflate, as exemplified by [^{11}C]NMSP, [^{11}C]flumazenil and [^{11}C]methionine. *Journal of Labelled Compounds and Radiopharmaceuticals*. 1998;41(9):831-841.

73. Jewett DM. A simple synthesis of [^{11}C]methyl triflate. *Int J Rad Appl Instrum A*. Nov 1992;43(11):1383-1385.

74. Dam JH, Bender D, Peters D, Nagren K. [^{11}C]NS9531, [^{11}C]NS9762 and [^{11}C]NS6417, specific SERT tracers: pre-clinical evaluation in pigs and optimization of synthesis conditions using [^{11}C]methyl triflate. *Nucl Med Biol*. Jan 2016;43(1):42-51.

75. Miller PW, Long NJ, de Mello AJ, Vilar R, Audrain H, Bender D, Passchier J, Gee A. Rapid multiphase carbonylation reactions by using a microtube reactor: applications in positron emission tomography 11C-radiolabeling. *Angew Chem Int Ed Engl*. 2007;46(16):2875-2878.

76. Fortt R, Gee A. Microfluidics: a golden opportunity for positron emission tomography? *Future Med Chem*. Mar 2013;5(3):241-244.

77. Krasikova RN, Andersson J, Truong P, Nag S, Shchukin EV, Halldin C. A fully automated one-pot synthesis of [carbonyl-^{11}C]WAY-100635 for clinical PET applications. *Appl Radiat Isot*. Jan 2009;67(1):73-78.

78. Christman DR, Finn RD, Karlstrom KI, Wolf AP. The production of ultra high activity ^{11}C-labeled hydrogen cyanide, carbon dioxide, carbon monoxide and methane

via the $^{14}N(p,\alpha)^{11}C$ reaction (XV). *The International Journal of Applied Radiation and Isotopes*. 1975;26(8):435-442.

79. Iwata R, Ido T, Takahashi T, Nakanishi H, Iida S. Optimization of [^{11}C]HCN production and no-carrier-added [^{11}C]amino acid synthesis. *Int J Rad Appl Instrum A*. 1987;38(2):97-102.

80. Långström B, Itsenko O, Rahman O. [^{11}C]Carbon monoxide, a versatile and useful precursor in labelling chemistry for PET-ligand development. *Journal of Labelled Compounds and Radiopharmaceuticals*. 2007;50(9-10):794-810.

81. Samuelsson L, Gottsater A, Lindgarde F. Decreasing levels of tumour necrosis factor alpha and interleukin 6 during lowering of body mass index with orlistat or placebo in obese subjects with cardiovascular risk factors. *Diabetes Obes Metab*. May 2003;5(3):195-201.

82. Huang Y, Narendran R, Bischoff Fo, Guo N, Zhu Z, Bae S-A, Lesage AS, Laruelle M. A Positron Emission Tomography Radioligand for the in Vivo Labeling of Metabotropic Glutamate 1 Receptor: (3-Ethyl-2-[^{11}C]methyl-6-quinolinyl)(cis- 4-methoxycyclohexyl)methanone. *Journal of Medicinal Chemistry*. 2005;48(16):5096-5099.

83. Wuest FR, Berndt M. ^{11}C–C bond formation by palladium-mediated cross-coupling of alkenylzirconocenes with [^{11}C]methyl iodide. *Journal of Labelled Compounds and Radiopharmaceuticals*. 2006;49(2):91-100.

84. Pauling L. The size of the molecule and thereby change the rates of *in vivo* absorption, while st. Nature of the Chemical Bond. *Cornell University Press: New York*. Feb 1940:189.

85. Snyder SE, Kilbourn MR. Handbook of Radiopharmaceuticals, Chapter 6: Chemistry of Fluorine-18 Radiopharmaceuticals;. *Wiley: New York*. 2009.

86. Smart BE. Fluorine substituent effects (on bioactivity). *Journal of Fluorine Chemistry*. 2001;109(1):3-11.

87. O´Hagan D, B. Harper D. Fluorine-containing natural products. *Journal of Fluorine Chemistry*. 1999;100(1-2):127-133.

88. Varrone A, Sjoholm N, Eriksson L, Gulyás B, Halldin C, Farde L. Advancement in PET quantification using 3D-OP-OSEM point spread function reconstruction with the HRRT. *Eur J Nucl Med Mol Imaging*. Oct 2009;36(10):1639-1650.

89. Nagy K, Tóth M, Major P, Patay G, Egri G, Häggkvist J, Varrone A, Farde L, Halldin C, Gulyás B. Performance evaluation of the small-animal nanoScan PET/MRI system. *J Nucl Med*. Oct 2013;54(10):1825-1832.

90. Schlyer DJ. PET tracers and radiochemistry. *Ann Acad Med Singapore*. Mar 2004;33(2):146-154.

91. Casella V, Ido T, Wolf AP, Fowler JS, MacGregor RR, Ruth TJ. Anhydrous ^{18}F-labeled eslemental flurine for radiopharmaceutical preparation. *J Nucl Med*. Aug 1980;21(8):750-757.

92. Palmer AJ, Clark JC, Goulding RW. The preparation of fluorine-18 labelled radiopharmaceuticals. *The International Journal of Applied Radiation and Isotopes*. 1977;28(12):53-65.

93. Nickles RJ, Gatley SJ, Votaw JR, Kornguth ML. Production of reactive fluorine-18. *Int J Rad Appl Instrum A*. 1986;37(8):649-661.

94. Nickles RJ, Daube ME, Ruth TJ. An $^{18}O_2$ target for the production of [^{18}F]F_2. *The International Journal of Applied Radiation and Isotopes*. 1984;35(2):117-122.

95. Hess E, Blessing G, Coenen HH, Qaim SM. Improved target system for production of high purity [^{18}F]fluorine via the ^{18}O(p,n)^{18}F reaction. *Applied Radiation and Isotopes*. 2000;52(6):1431-1440.

96. Chirakal R, Adams RM, Firnau G, Schrobilgen GJ, Coates G, Garnett ES. Electrophilic ^{18}F from a Siemens 11 MeV proton-only cyclotron. *Nucl Med Biol*. Jan 1995;22(1):111-116.

97. Bergman J, Solin O. Fluorine-18-labeled fluorine gas for synthesis of tracer molecules. *Nucl Med Biol*. Oct 1997;24(7):677-683.

98. Solin O, Bergman J, Haaparanta M, Reissell A. International Journal of Radiation Applications and Instrumentation. Part A. *Applied Radiation and Isotopes*. Feb 1988;39:1065-1071.

99. Schlyer DJ, Firouzbakht ML, Wolf AP. Impurities in the [^{18}O]water target and their effect on the yield of an aromatic displacement reaction with [^{18}F]fluoride. *Appl Radiat Isot*. Dec 1993;44(12):1459-1465.

100. Schlyer DJ, Bastos MA, Alexoff D, Wolf AP. Separation of [^{18}F]fluoride from [^{18}O]water using anion exchange resin. *Int J Rad Appl Instrum A*. 1990;41(6):531-533.

101. Coenen HH, Colosimo M, Schuller M, Stocklin G. Preparation of NCA [^{18}F]CH_2BrF via aminopolyether supported nucleophilic-substitution. *Journal of Labelled Compounds & Radiopharmaceuticals*. Jun 1986;23(6):587-595.

102. Kilbourn MR. Fluorine-18 labeling of radiopharmaceuticals. *Nuclear Science Series*. 1990;NAS-NS3203, National Academy Press, Washington, D.C.

103. Kiesewetter DO, Eckelman WC, Cohen RM, Finn RD, Larson SM. Syntheses and D2 receptor affinities of derivatives of spiperone containing aliphatic halogens. *Int J Rad Appl Instrum A*. 1986;37(12):1181-1188.

104. Hamacher K, Coenen HH, Stocklin G. Efficient stereospecific synthesis of no-carrier-added 2-[^{18}F]fluoro-2-deoxy-D-glucose using aminopolyether supported nucleophilic substitution. *J Nucl Med*. Feb 1986;27(2):235-238.

105. Brichard L, Aigbirhio FI. An Efficient Method for Enhancing the Reactivity and Flexibility of [^{18}F]Fluoride Towards Nucleophilic Substitution Using Tetraethylammonium Bicarbonate. *European Journal of Organic Chemistry*. 2014;2014(28):6145-6149.

106. Terrier F. Rate and equilibrium atudies in Jackson-Meisenheimer complexes. *Chemical Reviews*. 1982 1982;82(2):77-152.

107. Fernandez I, Frenking G, Uggerud E. Rate-Determining Factors in Nucleophilic Aromatic Substitution Reactions. *Journal of Organic Chemistry*. May 7 2010;75(9):2971-2980.

108. Kilbourn MR, Pavia MR, Gregor VE. Synthesis of fluorine-18 labeled GABA uptake inhibitors. *Int J Rad Appl Instrum A*. 1990;41(9):823-828.

109. Coenen HH, Kling P, Stocklin G. Cerebral metabolism of L-[^{18}F]fluorotyrosine, a new PET tracer of protein synthesis. *J Nucl Med*. Aug 1989;30(8):1367-1372.

110. Sun H, DiMagno SG. Competitive demethylation and substitution in N,N,N-trimethylanilinium fluorides. *Journal of Fluorine Chemistry*. Jul 2007;128(7):806-812.

111. McCarthy TJ, Sheriff AU, Graneto MJ, Talley JJ, Welch MJ. Radiosynthesis, in vitro validation, and in vivo evaluation of ^{18}F-labeled COX-1 and COX-2 inhibitors. *Journal of Nuclear Medicine*. Jan 2002;43(1):117-124.

112. Banks WR, Satter MR, Hwang DR. A new method for the NCA production of [^{18}F]Fluoromethane. *Applied Radiation and Isotopes*. Jan 1994;45(1):69-74.

113. Stephenson NA, Holland JP, Kassenbrock A, Yokell DL, Livni E, Liang SH, Vasdev N. Iodonium ylide-mediated radiofluorination of [^{18}F]FPEB and validation for human use. *J Nucl Med*. Mar 2015;56(3):489-492.

114. Dolle F. Fluorine-18-labelled fluoropyridines: advances in radiopharmaceutical design. *Curr Pharm Des*. 2005;11(25):3221-3235.

115. Simeon FG, Wendahl MT, Pike VW. The [^{18}F]2-fluoro-1,3-thiazolyl moiety-an easily-accessible structural motif for prospective molecular imaging radiotracers. *Tetrahedron Letters*. Nov 17 2010;51(46):6034-6036.

116. Simeon FG, Wendahl MT, Pike VW. Syntheses of 2-Amino and 2-Halothiazole Derivatives as High-Affinity Metabotropic Glutamate Receptor Subtype 5 Ligands and Potential Radioligands for in Vivo Imaging. *Journal of Medicinal Chemistry*. Feb 10 2011;54(3):901-908.

117. Carroll MA, Pike VW, Widdowson DA. New synthesis of diaryliodonium sulfonates from arylboronic acids. *Tetrahedron Letters*. Jul 2000;41(28):5393-5396.

118. Pike VW, Aigbirhio FI. Reactions of cyclotron-produced [^{18}F]fluoride with diaryliodonium salts-a novel single-step route to no-carrier-added [^{18}F]fluoroarenes. *Journal of the Chemical Society, Chemical Communications*. 1995(21):2215-2216.

119. Calderwood S, Collier TL, Gouverneur Vr, Liang SH, Vasdev N. Synthesis of [^{18}F]arenes from spirocyclic iodonium(III) ylides via continuous-flow microfluidics. *Journal of Fluorine Chemistry*. 2015;178:249-253.

120. Tredwell M, Gouverneur V. ^{18}F-labeling of arenes. *Angew Chem Int Ed Engl*. Nov 12 2012;51(46):11426-11437.

121. Block D, Coenen HH, Stöcklin G. N.C.A. [^{18}F]fluoroalkylation of H-acidic compounds. *Journal of Labelled Compounds and Radiopharmaceuticals*. 1988;25(2):201-216.

122. Kilbourn MR, Dence CS, Welch MJ, Mathias CJ. ^{18}F-Labeling of proteins. *Journal of Nuclear Medicine*. Apr 1987;28(4):462-470.

123. Block D, Coenen HH, Stöcklin G. N.C.A. ^{18}F-fluoroacylation via fluorocarboxylic acid esters. *Journal of Labelled Compounds and Radiopharmaceuticals*. 1988;25(2):185-200.

124. Shai Y, Kirk KL, Channing MA, Dunn BB, Lesniak MA, Eastman RC, Finn RD, Roth J, Jacobson KA. ^{18}F-labeled insulin:Aprosthetic group methodology for incorporation of a positron emitter into peptides and proteins. *Biochemistry*. May 30 1989;28(11):4801-4806.

125. Zhang M-R, Suzuki K. [^{18}F]fluoroalkyl agents: Synthesis, reactivity and application for development of PET ligands in molecular imaging. *Current Topics in Medicinal Chemistry*. 2007 2007;7(18):1817-1828.

126. Chi DY, Kilbourn MR, Katzenellenbogen JA, Brodack JW, Welch MJ. Synthesis of no-carrier-added N-([^{18}F]fluoroalkyl)spiperone derivatives. *Int J Rad Appl Instrum A*. 1986;37(12):1173-1180.

127. Iwata R, Pascali C, Bogni A, Furumoto S, Terasaki K, Yanai K. [^{18}F]fluoromethyl triflate, a novel and reactive [^{18}F]fluoromethylating agent: preparation and application to the on-column preparation of [^{18}F]fluorocholine. *Applied Radiation and Isotopes*. Sep 2002;57(3):347-352.

128. Chi DY, Kilbourn MR, Katzenellenbogen JA, Welch MJ. A rapid and efficient method for the fluoroalkylation of amines and amide-development of a method suitable for incorporation of the short-lived positron emitting radionuclide fluorine-18. *Journal of Organic Chemistry*. Feb 20 1987;52(4):658-664.

129. Bergman J, Eskola O, Lehikoinen P, Solin O. Automated synthesis and purification of [^{18}F]bromofluoromethane at high specific radioactivity. *Applied Radiation and Isotopes*. Jun 2001;54(6):927-933.

130. Spaeth N, Wyss MT, Weber B, Scheidegger S, Lutz A, Verwey J, Radovanovic I, Pahnke J, Wild D, Westera G, Weishaupt D, Hermann DM, Kaser-Hotz B, Aguzzi A, Buck A. Uptake of [^{18}F]fluorocholine, [^{18}F]fluoroethyl-*L*-tyrosine, and [^{18}F]FDG in acute cerebral radiation injury in the rat: Implications for separation of radiation necrosis from tumor recurrence. *Journal of Nuclear Medicine*. Nov 2004;45(11):1931-1938.

131. Wester HJ, Herz M, Weber W, Heiss P, Senekowitsch-Schmidtke R, Schwaiger M, Stocklin G. Synthesis and radiopharmacology of O-(2-[^{18}F]fluoroethyl)-L-tyrosine for tumor imaging. *Journal of Nuclear Medicine*. Jan 1999;40(1):205-212.

132. Kämäräinen E-L, Kyllönen T, Airaksinen A, Lundkvist C, Yu M, Någren K, Sandell J, Langer O, Vepsäläinen J, Hiltunen J, Bergström K, Lötjönen S, Jaakkola T, Halldin C. Preparation of [^{18}F]β-CFT-FP and [^{11}C]β-CFT-FP, selective radioligands for visualisation of the dopamine transporter using positron emission tomography (PET). *Journal of Labelled Compounds and Radiopharmaceuticals*. 2000;43(12):1235-1244.

133. Jacobson O, Chen X. PET designated flouride-18 production and chemistry. *Curr Top Med Chem*. 2010;10(11):1048-1059.

134. Bolton AE, Hunter WM. The labelling of proteins to high specific radioactivities by conjugation to a ^{125}I-containing acylating agent. *Biochem J*. Jul 1973;133(3):529-539.

135. Guhlke S, Wester HJ, Bruns C, Stocklin G. (2-[^{18}F]fluoropropionyl-(D)phe1)-octreotide, a potential radiopharmaceutical for quantitative somatostatin receptor imaging with PET: synthesis, radiolabeling, in vitro validation and biodistribution in mice. *Nucl Med Biol*. Aug 1994;21(6):819-825.

136. Vaidyanathan G, Zalutsky MR. Fluorine-18 labeled chemotactic peptides: a potential approach for the PET imaging of bacterial infection. *Nucl Med Biol*. Aug 1995;22(6):759-764.

137. Vaidyanathan G, Zalutsky MR. Improved synthesis of N-succinimidyl 4-[^{18}F]fluorobenzoate and its application to the labeling of a monoclonal-antibody fragment. *Bioconjugate Chemistry*. Jul-Aug 1994;5(4):352-356.

138. Lang L, Eckelman WC. One-step synthesis of ^{18}F labeled [^{18}F]-N-succinimidyl 4-(fluoromethyl)benzoate for protein labeling. *Appl Radiat Isot*. Dec 1994;45(12):1155-1163.

139. Lang L, Eckelman WC. Labeling proteins at high specific activity using N-succinimidyl 4-[^{18}F](fluoromethyl) benzoate. *Appl Radiat Isot*. Feb 1997;48(2):169-173.

140. Li W, Lang L, Niu G, Guo N, Ma Y, Kiesewetter DO, Shen B, Chen X. N-Succinimidyl 4-[^{18}F]-fluoromethylbenzoate-labeled dimeric RGD peptide for imaging tumor integrin expression. *Amino acids*. 2012;43(3):1349-1357.

141. McBride WJ, Sharkey RM, Karacay H, D'Souza CA, Rossi EA, Laverman P, Chang CH, Boerman OC, Goldenberg DM. A novel method of 18F radiolabeling for PET. *J Nucl Med*. Jun 2009;50(6):991-998.

142. Chitneni SK, Serdons K, Evens N, Fonge H, Celen S, Deroose CM, Debyser Z, Mortelmans L, Verbruggen AM, Bormans GM. Efficient purification and metabolite analysis of radiotracers using high-performance liquid chromatography and on-line solid-phase extraction. *J Chromatogr A*. May 2 2008;1189(1-2):323-331.

143. Serdons K, Verbruggen A, Bormans G. The presence of ethanol in radiopharmaceutical injections. *J Nucl Med*. Dec 2008;49(12):2071.

144. Scott PJ, Hockley BG, Kung HF, Manchanda R, Zhang W, Kilbourn MR. Studies into radiolytic decomposition of fluorine-18 labeled radiopharmaceuticals for positron emission tomography. *Appl Radiat Isot*. Jan 2009;67(1):88-94.

145. Beyer T, Townsend DW, Brun T, Kinahan PE, Charron M, Roddy R, Jerin J, Young J, Byars L, Nutt R. A combined PET/CT scanner for clinical oncology. *J Nucl Med*. Aug 2000;41(8):1369-1379.

146. Brissova M, Fowler MJ, Nicholson WE, Chu A, Hirshberg B, Harlan DM, Powers AC. Assessment of human pancreatic islet architecture and composition by laser scanning confocal microscopy. *J Histochem Cytochem*. Sep 2005;53(9):1087-1097.

147. Bosco D, Armanet M, Morel P, Niclauss N, Sgroi A, Muller YD, Giovannoni L, Parnaud G, Berney T. Unique arrangement of alpha- and beta-cells in human islets of Langerhans. *Diabetes*. May 2010;59(5):1202-1210.

148. Rahier J, Guiot Y, Goebbels RM, Sempoux C, Henquin JC. Pancreatic beta-cell mass in European subjects with type 2 diabetes. *Diabetes Obes Metab*. Nov 2008;10 Suppl 4:32-42.

149. Klein T, Fujii M, Sandel J, Shibazaki Y, Wakamatsu K, Mark M, Yoneyama H. Linagliptin alleviates hepatic steatosis and inflammation in a mouse model of non-alcoholic steatohepatitis. *Med Mol Morphol*. Sep 2014;47(3):137-149.

150. Scully T. Demography: To the limit. *Nature*. Dec 6 2012;492(7427):S2-3.

151. Gepts W. Pathologic anatomy of the pancreas in juvenile diabetes mellitus. *Diabetes*. Oct 1965;14(10):619-633.

152. Butler AE, Janson J, Bonner-Weir S, Ritzel R, Rizza RA, Butler PC. Beta-cell deficit and increased beta-cell apoptosis in humans with type 2 diabetes. *Diabetes*. Jan 2003;52(1):102-110.

153. Melendez-Ramirez LY, Richards RJ, Cefalu WT. Complications of type 1 diabetes. *Endocrinol Metab Clin North Am*. Sep 2010;39(3):625-640.

154. Smith-Spangler CM, Bhattacharya J, Goldhaber-Fiebert JD. Diabetes, its treatment, and catastrophic medical spending in 35 developing countries. *Diabetes Care*. Feb 2012;35(2):319-326.

155. Selvaraju RK. [^{68}Ga]Exendin-4: Bench-to-Bedside: PET molecular imaging of the GLP-1 receptor for diabetes and cancer. *Digital Comprehensive Summaries of Uppsala Dissertations from the Faculty of Pharmacy*. 2015(202).

156. Matveyenko AV, Butler PC. Relationship between beta-cell mass and diabetes onset. *Diabetes Obes Metab*. Nov 2008;10 Suppl 4:23-31.

157. Krogvold L, Edwin B, Buanes T, Frisk G, Skog O, Anagandula M, Korsgren O, Undlien D, Eike MC, Richardson SJ, Leete P, Morgan NG, Oikarinen S, Oikarinen M, Laiho JE, Hyoty H, Ludvigsson J, Hanssen KF, Dahl-Jorgensen K. Detection of a low-grade enteroviral infection in the islets of langerhans of living patients newly diagnosed with type 1 diabetes. *Diabetes*. May 2015;64(5):1682-1687.

158. Eriksson O, Laughlin M, Brom M, Nuutila P, Roden M, Hwa A, Bonadonna R, Gotthardt M. In vivo imaging of beta cells with radiotracers: state of the art, prospects and recommendations for development and use. *Diabetologia*. Jul 2016;59(7):1340-1349.

159. Sherry NA, Tsai EB, Herold KC. Natural history of beta-cell function in type 1 diabetes. *Diabetes*. Dec 2005;54 Suppl 2:S32-39.

160. Harris MI. Epidemiologic studies on the pathogenesis of non-insulin-dependent diabetes mellitus (NIDDM). *Clin Invest Med*. Aug 1995;18(4):231-239.

161. Goland R, Freeby M, Parsey R, Saisho Y, Kumar D, Simpson N, Hirsch J, Prince M, Maffei A, Mann JJ, Butler PC, Van Heertum R, Leibel RL, Ichise M, Harris PE. ^{11}C-dihydrotetrabenazine PET of the pancreas in subjects with long-standing type 1 diabetes and in healthy controls. *J Nucl Med*. Mar 2009;50(3):382-389.

162. Normandin MD, Petersen KF, Ding YS, Lin SF, Naik S, Fowles K, Skovronsky DM, Herold KC, McCarthy TJ, Calle RA, Carson RE, Treadway JL, Cline GW. In vivo imaging of endogenous pancreatic beta-cell mass in healthy and type 1 diabetic subjects using [^{18}F]fluoropropyl-dihydrotetrabenazine and PET. *J Nucl Med*. Jun 2012;53(6):908-916.

163. Freeby MJ, Kringas P, Goland RS, Leibel RL, Maffei A, Divgi C, Ichise M, Harris PE. Cross-sectional and Test-Retest Characterization of PET with [^{18}F]FP-(+)-DTBZ for beta Cell Mass Estimates in Diabetes. *Mol Imaging Biol*. Apr 2016;18(2):292-301.

164. Selvaraju RK, Bulenga TN, Espes D, Lubberink M, Sorensen J, Eriksson B, Estrada S, Velikyan I, Eriksson O. Dosimetry of [^{68}Ga]Ga-DO3A-VS-Cys(40)-Exendin-4 in rodents, pigs, non-human primates and human - repeated scanning in human is possible. *Am J Nucl Med Mol Imaging*. 2015;5(3):259-269.

165. Eriksson O, Espes D, Selvaraju RK, Jansson E, Antoni G, Sorensen J, Lubberink M, Biglarnia AR, Eriksson JW, Sundin A, Ahlstrom H, Eriksson B, Johansson L, Carlsson PO, Korsgren O. Positron emission tomography ligand [^{11}C]5-hydroxy-tryptophan can be used as a surrogate marker for the human endocrine pancreas. *Diabetes*. Oct 2014;63(10):3428-3437.

166. Sweet IR, Cook DL, Lernmark A, Greenbaum CJ, Krohn KA. Non-invasive imaging of beta cell mass: a quantitative analysis. *Diabetes Technol Ther*. Oct 2004;6(5):652-659.

167. Blomberg BA, Codreanu I, Cheng G, Werner TJ, Alavi A. Beta-cell imaging: call for evidence-based and scientific approach. *Mol Imaging Biol*. Apr 2013;15(2):123-130.

168. Laurent D, Vinet L, Lamprianou S, Daval M, Filhoulaud G, Ktorza A, Wang H, Sewing S, Juretschke HP, Glombik H, Meda P, Boisgard R, Nguyen DL, Stasiuk GJ, Long NJ, Montet X, Hecht P, Kramer W, Rutter GA, Hecksher-Sorensen J. Pancreatic beta-cell imaging in humans: fiction or option? *Diabetes Obes Metab*. Jan 2016;18(1):6-15.

169. Hebert LE, Scherr PA, Bienias JL, Bennett DA, Evans DA. Alzheimer disease in the US population: prevalence estimates using the 2000 census. *Arch Neurol*. Aug 2003;60(8):1119-1122.

170. Davis KL, Samuels SC. Pharmacological Management of Neurological and Psychiatric Disorders Pharmacological Management of Neurological and Psychiatric Disorders *McGraw-Hill, New York*. Sep 1998:267-316.

171. Hardy J, Selkoe DJ. The amyloid hypothesis of Alzheimer's disease: progress and problems on the road to therapeutics. *Science*. Jul 19 2002;297(5580):353-356.

172. Hardy JA, Higgins GA. Alzheimer's disease: the amyloid cascade hypothesis. *Science*. Apr 10 1992;256(5054):184-185.

173. Braak H, Braak E. Diagnostic criteria for neuropathologic assessment of Alzheimer's disease. *Neurobiol Aging*. Jul-Aug 1997;18(4 Suppl):S85-88.

174. Ferri CP, Prince M, Brayne C, Brodaty H, Fratiglioni L, Ganguli M, Hall K, Hasegawa K, Hendrie H, Huang Y, Jorm A, Mathers C, Menezes PR, Rimmer E, Scazufca M. Global prevalence of dementia: a Delphi consensus study. *Lancet*. Dec 17 2005;366(9503):2112-2117.

175. Klunk WE, Engler H, Nordberg A, Wang Y, Blomqvist G, Holt DP, Bergström M, Savitcheva I, Huang GF, Estrada S, Ausen B, Debnath ML, Barletta J, Price JC, Sandell J, Lopresti BJ, Wall A, Koivisto P, Antoni G, Mathis CA, Långström B. Imaging brain amyloid in Alzheimer's disease with Pittsburgh Compound-B. *Ann Neurol*. Mar 2004;55(3):306-319.

176. Mathis CA, Wang Y, Holt DP, Huang GF, Debnath ML, Klunk WE. Synthesis and evaluation of ^{11}C-labeled 6-substituted 2-arylbenzothiazoles as amyloid imaging agents. *J Med Chem*. Jun 19 2003;46(13):2740-2754.

177. Johnson AE, Jeppsson F, Sandell J, Wensbo D, Neelissen JA, Jureus A, Strom P, Norman H, Farde L, Svensson SP. AZD2184: a radioligand for sensitive detection of beta-amyloid deposits. *J Neurochem*. Mar 2009;108(5):1177-1186.

178. Nyberg S, Jonhagen ME, Cselenyi Z, Halldin C, Julin P, Olsson H, Freund-Levi Y, Andersson J, Varnas K, Svensson S, Farde L. Detection of amyloid in Alzheimer's disease with positron emission tomography using [^{11}C]AZD2184. *Eur J Nucl Med Mol Imaging*. Nov 2009;36(11):1859-1863.

179. Koole M, Lewis DM, Buckley C, Nelissen N, Vandenbulcke M, Brooks DJ, Vandenberghe R, Van Laere K. Whole-body biodistribution and radiation dosimetry of [^{18}F]GE067: a radioligand for in vivo brain amyloid imaging. *J Nucl Med*. May 2009;50(5):818-822.

180. Nelissen N, Van Laere K, Thurfjell L, Owenius R, Vandenbulcke M, Koole M, Bormans G, Brooks DJ, Vandenberghe R. Phase 1 study of the Pittsburgh compound

B derivative [^{18}F]flutemetamol in healthy volunteers and patients with probable Alzheimer disease. *J Nucl Med*. Aug 2009;50(8):1251-1259.

181. Cselenyi Z, Jonhagen ME, Forsberg A, Halldin C, Julin P, Schou M, Johnstrom P, Varnas K, Svensson S, Farde L. Clinical validation of [^{18}F]AZD4694, an amyloid-beta-specific PET radioligand. *J Nucl Med*. Mar 2012;53(3):415-424.

182. Zhang W, Oya S, Kung MP, Hou C, Maier DL, Kung HF. F-18 Polyethyleneglycol stilbenes as PET imaging agents targeting Abeta aggregates in the brain. *Nucl Med Biol*. Nov 2005;32(8):799-809.

183. Rowe CC, Ackerman U, Browne W, Mulligan R, Pike KL, O'Keefe G, Tochon-Danguy H, Chan G, Berlangieri SU, Jones G, Dickinson-Rowe KL, Kung HP, Zhang W, Kung MP, Skovronsky D, Dyrks T, Holl G, Krause S, Friebe M, Lehman L, Lindemann S, Dinkelborg LM, Masters CL, Villemagne VL. Imaging of amyloid beta in Alzheimer's disease with ^{18}F-BAY94-9172, a novel PET tracer: proof of mechanism. *Lancet Neurol*. Feb 2008;7(2):129-135.

184. Zhang W, Kung MP, Oya S, Hou C, Kung HF. ^{18}F-labeled styrylpyridines as PET agents for amyloid plaque imaging. *Nucl Med Biol*. Jan 2007;34(1):89-97.

185. Choi SR, Golding G, Zhuang Z, Zhang W, Lim N, Hefti F, Benedum TE, Kilbourn MR, Skovronsky D, Kung HF. Preclinical properties of ^{18}F-AV-45: a PET agent for Abeta plaques in the brain. *J Nucl Med*. Nov 2009;50(11):1887-1894.

186. Kung HF. The beta-Amyloid Hypothesis in Alzheimer's Disease: Seeing Is Believing. *ACS Med Chem Lett*. Apr 12 2012;3(4):265-267.

187. Hampel H, Burger K, Teipel SJ, Bokde AL, Zetterberg H, Blennow K. Core candidate neurochemical and imaging biomarkers of Alzheimer's disease. *Alzheimers Dement*. Jan 2008;4(1):38-48.

188. Någren K, Muller L, Halldin C, Swahn CG, Lehikoinen P. Improved synthesis of some commonly used PET radioligands by the use of [^{11}C]methyl triflate. *Nucl Med Biol*. Feb 1995;22(2):235-239.

189. Guillaume M, Luxen A, Nebeling B, Argentini M, Clark JC, Pike VW. Recommendation for F-18 production. *Applied Radiation and Isotopes*. 1991;42(8):749-762.

190. Gomzina NA, Vasil'ev DA, Krasikova RN. Optimization of Automated Synthesis of 2-[^{18}F]Fluoro-2-deoxy-D-glucose Involving Base Hydrolysis. *Radiochemistry*. 2002/07/01 2002;44(4):403-409.

191. Tang G, Zeng W, Yu M, Kabalka G. Facile synthesis of N-succinimidyl 4-[^{18}F]fluorobenzoate ([^{18}F]SFB) for protein labeling. *Journal of Labelled Compounds and Radiopharmaceuticals*. 2008;51(1):68-71.

192. Johnström P, Clark JC, Pickard JD, Davenport AP. Automated synthesis of the generic peptide labelling agent N-succinimidyl 4-[^{18}F]fluorobenzoate and application to (18)F-label the vasoactive transmitter urotensin-II as a ligand for positron emission tomography. *Nucl Med Biol*. Aug 2008;35(6):725-731.

193. Hall H, Hurd Y, Pauli S, Halldin C, Sedvall G. Human brain imaging post-mortem - whole hemisphere technologies. *International Review of Psychiatry*. Feb 2001;13(1):12-17.

194. Hall H, Halldin C, Farde L, Sedvall G. Whole hemisphere autoradiography of the postmortem human brain. *Nuclear Medicine and Biology*. Nov 1998;25(8):715-719.

195. Goto M, Eich TM, Felldin M, Foss A, Kallen R, Salmela K, Tibell A, Tufveson G, Fujimori K, Engkvist M, Korsgren O. Refinement of the automated method for human islet isolation and presentation of a closed system for in vitro islet culture. *Transplantation*. Nov 15 2004;78(9):1367-1375.

196. Clark JD, Gebhart GF, Gonder JC, Keeling ME, Kohn DF. Special Report: The 1996 Guide for the Care and Use of Laboratory Animals. *ILAR J*. 1997;38(1):41-48.

197. Anlauf M, Eissele R, Schafer MK, Eiden LE, Arnold R, Pauser U, Kloppel G, Weihe E. Expression of the two isoforms of the vesicular monoamine transporter (VMAT1 and VMAT2) in the endocrine pancreas and pancreatic endocrine tumors. *J Histochem Cytochem*. Aug 2003;51(8):1027-1040.

198. Goswami R, Ponde DE, Kung MP, Hou C, Kilbourn MR, Kung HF. Fluoroalkyl derivatives of dihydrotetrabenazine as positron emission tomography imaging agents targeting vesicular monoamine transporters. *Nucl Med Biol*. Aug 2006;33(6):685-694.

199. Kung HF, Lieberman BP, Zhuang ZP, Oya S, Kung MP, Choi SR, Poessl K, Blankemeyer E, Hou C, Skovronsky D, Kilbourn M. In vivo imaging of vesicular monoamine transporter 2 in pancreas using an ^{18}F-epoxide derivative of tetrabenazine. *Nucl Med Biol*. Nov 2008;35(8):825-837.

200. Tsao HH, Lin KJ, Juang JH, Skovronsky DM, Yen TC, Wey SP, Kung MP. Binding characteristics of 9-fluoropropyl-(+)-dihydrotetrabenzazine (AV-133) to the vesicular monoamine transporter type 2 in rats. *Nucl Med Biol*. May 2010;37(4):413-419.

201. Kung MP, Hou C, Lieberman BP, Oya S, Ponde DE, Blankemeyer E, Skovronsky D, Kilbourn MR, Kung HF. In vivo imaging of beta-cell mass in rats using [^{18}F]-FP-(+)-DTBZ: a potential PET ligand for studying diabetes mellitus. *J Nucl Med*. Jul 2008;49(7):1171-1176.

202. Eriksson O, Jahan M, Johnström P, Korsgren O, Sundin A, Halldin C, Johansson L. In vivo and in vitro characterization of [^{18}F]FE-(+)-DTBZ as a tracer for beta-cell mass. *Nucl Med Biol*. Apr 2010;37(3):357-363.

203. Zhang MR, Tsuchiyama A, Haradahira T, Yoshida Y, Furutsuka K, Suzuki K. Development of an automated system for synthesizing ^{18}F-labeled compounds using [^{18}F]fluoroethyl bromide as a synthetic precursor. *Appl Radiat Isot*. Sep 2002;57(3):335-342.

204. Matschinsky FM, Ellerman JE. Metabolism of glucose in the islets of Langerhans. *J Biol Chem*. May 25 1968;243(10):2730-2736.

205. Walker DG, Rao S. The role of glucokinase in the phosphorylation of glucose by rat liver. *Biochem J*. Feb 1964;90(2):360-368.

206. Kamata K, Mitsuya M, Nishimura T, Eiki J, Nagata Y. Structural basis for allosteric regulation of the monomeric allosteric enzyme human glucokinase. *Structure*. Mar 2004;12(3):429-438.

207. Grimsby J, Sarabu R, Corbett WL, Haynes NE, Bizzarro FT, Coffey JW, Guertin KR, Hilliard DW, Kester RF, Mahaney PE, Marcus L, Qi L, Spence CL, Tengi J, Magnuson MA, Chu CA, Dvorozniak MT, Matschinsky FM, Grippo JF. Allosteric activators of glucokinase: potential role in diabetes therapy. *Science*. Jul 18 2003;301(5631):370-373.

208. Matschinsky FM. Assessing the potential of glucokinase activators in diabetes therapy. *Nat Rev Drug Discov*. May 2009;8(5):399-416.

209. Lindskog C, Korsgren O, Ponten F, Eriksson JW, Johansson L, Danielsson A. Novel pancreatic beta cell-specific proteins: antibody-based proteomics for identification of new biomarker candidates. *J Proteomics*. May 17 2012;75(9):2611-2620.

210. Pearson RG, Songstad J. Application of the Principle of Hard and Soft Acids and Bases to Organic Chemistry. *Journal of the American Chemical Society*. 1967;89(8):1827-1836.

211. Meek JS, Fowler JS. Photolysis and pyrolysis of trans-azidovinyl p-tolyl sulfone. *The Journal of Organic Chemistry*. 1968;33(9):3418-3421.

212. Funke SA, Willbold D. Mirror image phage display--a method to generate D-peptide ligands for use in diagnostic or therapeutical applications. *Mol Biosyst*. Aug 2009;5(8):783-786.

213. Wiesehan K, Buder K, Linke RP, Patt S, Stoldt M, Unger E, Schmitt B, Bucci E, Willbold D. Selection of D-amino-acid peptides that bind to Alzheimer's disease amyloid peptide abeta1-42 by mirror image phage display. *Chembiochem*. Aug 4 2003;4(8):748-753.

214. Funke SA, Birkmann E, Willbold D. Detection of Amyloid-beta aggregates in body fluids: a suitable method for early diagnosis of Alzheimer's disease? *Curr Alzheimer Res*. Jun 2009;6(3):285-289.

215. Van Groen T, Kadish I, Wiesehan K, Funke SA, Willbold D. In vitro and in vivo staining characteristics of small, fluorescent, Abeta42-binding D-enantiomeric peptides in transgenic AD mouse models. *ChemMedChem*. Feb 2009;4(2):276-282.

216. Wiesehan K, Stohr J, Nagel-Steger L, van Groen T, Riesner D, Willbold D. Inhibition of cytotoxicity and amyloid fibril formation by a D-amino acid peptide that specifically binds to Alzheimer's disease amyloid peptide. *Protein Eng Des Sel*. Apr 2008;21(4):241-246.

217. Schumacher TNM, Mayr LM, Minor DL, Milhollen MA, Burgess MW, Kim PS. Identification of D-peptide ligands through mirror-image phage display. *Science*. Mar 29 1996;271(5257):1854-1857.

218. Herve M, Maillere B, Mourier G, Texier C, Leroy S, Menez A. On the immunogenic properties of retro-inverso peptides. Total retro-inversion of T-cell epitopes causes a loss of binding to MHC II molecules. *Molecular Immunology*. Feb 1997;34(2):157-163.

219. Eckert DM, Malashkevich VN, Hong LH, Carr PA, Kim PS. Inhibiting HIV-1 entry: Discovery of D-peptide inhibitors that target the gp41 coiled-coil pocket. *Cell*. Oct 1 1999;99(1):103-115.

220. Zawadzke LE, Berg JM. A Racemic Protein. *Journal of the American Chemical Society*. May 6 1992;114(10):4002-4003.

221. Poduslo JF, Curran GL, Kumar A, Frangione B, Soto C. beta-sheet breaker peptide inhibitor of Alzheimer's amyloidogenesis with increased blood-brain barrier permeability and resistance to proteolytic degradation in plasma. *Journal of Neurobiology*. Jun 5 1999;39(3):371-382.

222. Findeis MA, Musso GM, Arico-Muendel CC, Benjamin HW, Hundal AM, Lee JJ, Chin J, Kelley M, Wakefield J, Hayward NJ, Molineaux SM. Modified-peptide inhibitors of amyloid beta-peptide polymerization. *Biochemistry*. May 25 1999;38(21):6791-6800.

223. Dintzis HM, Symer DE, Dintzis RZ, Zawadzke LE, Berg JM. A comparison of the immunogenicity of a pair of enantiomeric proteins. *Proteins-Structure Function and Genetics*. Jul 1993;16(3):306-308.

224. Johnström P, Harris NG, Fryer TD, Barret O, Clark JC, Pickard JD, Davenport AP. ^{18}F-Endothelin-1, a positron emission tomography (PET) radioligand for the endothelin receptor system: radiosynthesis and in vivo imaging using microPET. *Clinical Science*. Aug 2002;103:4S-8S.

225. Haka MS, Kilbourn MR, Watkins GL, Toorongian SA. Aryltrimethylammonium trifluoromethanesulfonates as precursors to aryl [^{18}F]fluorides-improved synthesis of Aryltrimethylammonium trifluoromethanesulfonates as precursors to aryl [^{18}F]fluorides-improved synthesis of [^{18}F]GBR-13119. *Journal of Labelled Compounds & Radiopharmaceuticals*. Jul 1989;27(7):823-833.

226. Johnström P, Clark JC, Pickard JD, Davenport AP. Automated synthesis of the generic peptide labelling agent N-succinimidyl 4-[^{18}F]fluorobenzoate and application to ^{18}F-label the vasoactive transmitter urotensin-II as a ligand for positron emission tomography. *Nuclear Medicine and Biology*. Aug 2008;35(6):725-731.

227. Tang G, Zeng W, Yu M, Kabalka G. Facile synthesis of N-succinimidyl 4-[^{18}F]fluorobenzoate ([^{18}F]SFB) for protein labeling. *Journal of Labelled Compounds & Radiopharmaceuticals*. Jan-Feb 2008;51(1-2):68-71.

228. Bonner-Weir S. Regulation of pancreatic beta-cell mass in vivo. *Recent Prog Horm Res*. 1994;49:91-104.

229. Nalin L, Selvaraju RK, Velikyan I, Berglund M, Andreasson S, Wikstrand A, Ryden A, Lubberink M, Kandeel F, Nyman G, Korsgren O, Eriksson O, Jensen-Waern M. Positron emission tomography imaging of the glucagon-like peptide-1 receptor in healthy and streptozotocin-induced diabetic pigs. *Eur J Nucl Med Mol Imaging*. Sep 2014;41(9):1800-1810.